JGR Solid Earth

RESEARCH ARTICLE
10.1029/2024JB028692

Key Points:

- At typical slip variability, the geomorphic record does not resolve more than two paleo-slip distributions, except under specific conditions
- Low slip variability, high slip-per-event, and semiarid conditions increase the likelihood of recording more than two slip distributions
- Characteristic slip may be less common than implied by the geomorphic record

Supporting Information:

Supporting Information may be found in the online version of this article.

Correspondence to:

N. G. Reitman,
nreitman@usgs.gov

Citation:

Reitman, N. G., Klinger, Y., Briggs, R. W., & Gold, R. D. (2024). Limited preservation of strike-slip surface displacement in the geomorphic record. *Journal of Geophysical Research: Solid Earth*, *129*, e2024JB028692. https://doi.org/10.1029/2024JB028692

Received 8 JAN 2024
Accepted 5 NOV 2024

Author Contributions:

Conceptualization: Nadine G. Reitman, Yann Klinger, Richard W. Briggs, Ryan D. Gold
Data curation: Nadine G. Reitman
Formal analysis: Nadine G. Reitman
Funding acquisition: Nadine G. Reitman, Yann Klinger
Investigation: Nadine G. Reitman
Methodology: Nadine G. Reitman
Project administration: Nadine G. Reitman
Resources: Nadine G. Reitman
Software: Nadine G. Reitman
Supervision: Yann Klinger, Richard W. Briggs, Ryan D. Gold
Validation: Nadine G. Reitman
Visualization: Nadine G. Reitman
Writing – original draft: Nadine G. Reitman
Writing – review & editing: Nadine G. Reitman, Yann Klinger, Richard W. Briggs, Ryan D. Gold

Limited Preservation of Strike-Slip Surface Displacement in the Geomorphic Record

Nadine G. Reitman[1], Yann Klinger[2], Richard W. Briggs[1], and Ryan D. Gold[1]

[1]U.S. Geological Survey, Geologic Hazards Science Center, Golden, CO, USA, [2]Université de Paris Cité, Institut de Physique du Globe de Paris, CNRS, Paris, France

Abstract Offset geomorphic markers are commonly used to interpret slip history of strike-slip faults and have played an important role in forming earthquake recurrence models. These data sets are typically analyzed using cumulative probability methods to interpret average amounts of slip in past earthquakes. However, interpretation of the geomorphic record to infer surface slip history is complicated by slip variability, measurement uncertainty, and modification of offset features in the landscape. To investigate how well geomorphic data record surface slip, we use offset measurements from recent strike-slip surface ruptures ($n = 39$), faults with geomorphic evidence of multiple strike-slip earthquakes ($n = 29$), and synthetic slip distributions with added noise (n>10,000) to examine the constraints of the geomorphic record and the underlying assumptions of the cumulative offset probability distribution analysis method. We find that the geomorphic record is unlikely to resolve more than two paleo-slip distributions, except in specific cases with low slip variability, high slip-per-event, and semiarid climate. In cases where site-specific conditions allow for interpretation of more than two earthquakes, lateral extrapolation along a fault is not straightforward because on-fault displacement and distributed deformation may be spatially variable in each earthquake. We also find that average slip in modern earthquakes is adequately recovered by probability methods, but the reported prevalence of strike-slip faults with characteristic slip history is not supported by geomorphic data. We also propose updated methods to interpret slip history and construct uncertainty bounds for paleo-slip distributions.

Plain Language Summary Earthquake history on strike-slip faults is often interpreted from landforms (e.g., small channels) displaced across a fault that record different amounts of slip depending on how many earthquakes they have experienced. These data sets of displaced landforms are typically analyzed using probability methods to interpret the history of slip on a fault. However, from modern earthquakes, we know that earthquakes have complex surface slip patterns, and the geomorphic record of surface slip is modified by precipitation and anthropogenic activities after an earthquake. To investigate how well geomorphic data record surface slip, we use displaced landform data from modern earthquakes, faults with geomorphic evidence of multiple earthquakes, and synthetic data sets to examine the underlying assumptions in the typical analysis methods and how characteristics of surface slip (slip variability, data density, slip distribution shape, slip amplitude, and slip history) affect how to interpret earthquake history from geomorphic data. We find that the geomorphic record stores less information than previously thought, rarely more than two earthquakes, and we propose updated methods to interpret geomorphic data from strike-slip faults.

1. Introduction

The geomorphic record stores information about past earthquakes and offers one of the few methods of assessing the ∼1–100 kyr record of slip, which is used to determine the probabilistic hazard posed by active faults on human timescales. Geomorphic markers (e.g., stream channels) displaced across strike-slip faults measured in the hours to centuries after an earthquake form the basis of slip distributions (e.g., Haeussler et al., 2004; Lindvall et al., 1989; Zielke et al., 2012), which have been used to formulate earthquake recurrence models (Schwartz & Coppersmith, 1984; Sieh, 1996) and fault displacement models (e.g., Baize et al., 2019; Petersen et al., 2011). However, the geomorphic record integrates both tectonic and climatic signals (e.g., Reitman et al., 2023; Wallace, 1968; Zielke, 2018), and thus must be interpreted carefully to extract robust information. With the proliferation of high-resolution geomorphic data available via lidar, satellite imagery, and drone surveys, quantitative evaluation of how well surface slip with different characteristics (e.g., slip variability, slip amplitude, slip distribution, slip history) is stored in the geomorphic record is vital to make interpretations that inform earthquake hazard.

10.1029/2024JB028692

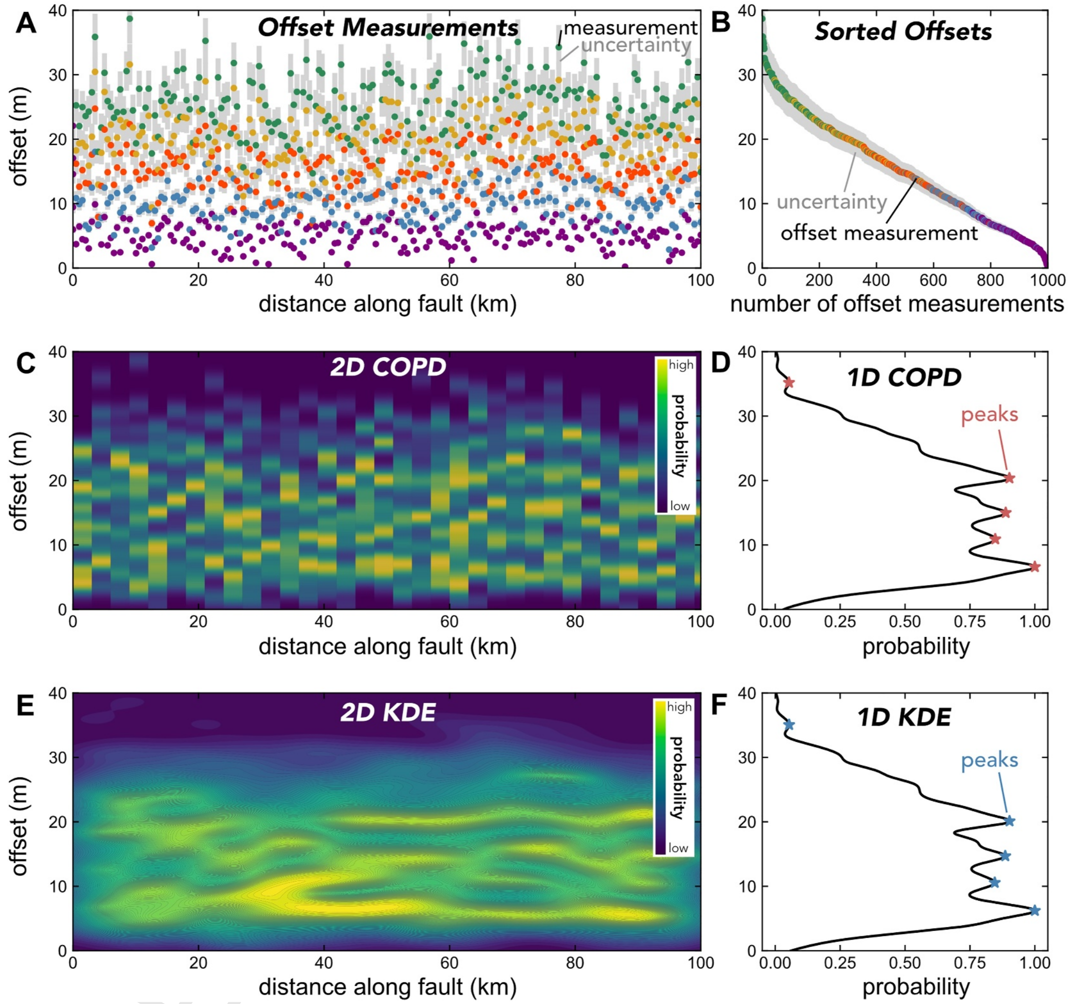

Figure 1. Example application of cumulative offset probability distribution (COPD) analysis of a synthetic data set with five 5-m-slip earthquakes and 30% noise. (a) Offset measurements (colored circles) with uncertainty (gray bars) plotted by distance along the fault. Each color represents a different earthquake. (b) Offset measurements and uncertainty ranges sorted from largest to smallest. (c) Two-dimensional cumulative offset probability distribution (2D COPD) of the offset measurements calculated with 3-km spatial bins and Gaussian probability density functions (PDFs) for each measurement. (d) One-dimensional (1D) COPD with peaks selected by an automatic peak finding algorithm. (e) 2D kernel density estimate (KDE) of the offset measurements. (f) 1D KDE, which has a similar shape and peak values to the 1D COPD. Peaks in the 1D COPD and KDE are interpreted as cumulative slip in past earthquakes, and slip-per-event and coefficient of variation (CV) of slip-per-event are derived from the peak heights.

For strike-slip faults, the geomorphic record of surface-rupturing earthquakes is commonly analyzed using data sets of geomorphic markers offset across the fault (e.g., Zielke et al., 2015). Geomorphic markers created at different times record varying amounts of slip depending on how many earthquakes have displaced them (e.g., Grant Ludwig et al., 2010; Zielke et al., 2010). These data sets are typically interpreted using probability methods in which a probability density function (PDF) between an uncertainty range is constructed for each offset measurement, and the PDFs all offset measurements for a fault or fault section are summed into an aggregate density function, termed the cumulative offset probability distribution (COPD) (Figure 1) (e.g., Klinger et al., 2000; McGill & Sieh, 1991; Zielke et al., 2010, 2015). The peaks in the distribution, which are the modal offset values, are often interpreted to represent amounts of slip in individual past earthquakes (e.g., Klinger et al., 2011; McGill & Sieh, 1991), although peaks can integrate slip from multiple earthquakes (e.g., Zielke et al., 2012). The most recent earthquake (MRE) commonly has the highest peak followed by an exponential decay in peak heights (e.g., Klinger et al., 2011; Zielke et al., 2010). Assumptions inherent to the COPD method are that the modal offset value corresponds with average slip-per-event, slip variability within a studied fault section is minimal, and fault sections can be interpreted from offset recorded by geomorphic markers or fault structure.

Modern strike-slip earthquakes (i.e., recent and historical) highlight some of the factors that make past surface slip challenging to reconstruct from offset geomorphic markers. First, surface slip along a ruptured fault or fault section can be variable (e.g., R. D. Gold et al., 2015; Haeussler et al., 2004; Lin et al., 2020; Rockwell & Klinger, 2013; Reitman, Mueller, & Tucker, 2022), even within short distances along strike (e.g., DuRoss et al., 2020; McGill & Sieh, 1991; Rockwell et al., 2002). Second, distributed deformation (i.e., deformation 100 m to 1 km from the primary fault trace) can be ∼15%–50% of total surface slip (Antoine et al., 2021; R. D. Gold et al., 2015, 2021; Milliner et al., 2015; Rockwell et al., 2002; Vallage et al., 2015) and can vary at short length scales along a surface rupture (e.g., Antoine et al., 2021; Milliner et al., 2015; Rockwell et al., 2002; Zinke et al., 2014). Third, rupture end points commonly spill over structural complexities, discontinuities, or fault section boundaries (e.g., Schwartz, 2018; Wesnousky, 2006). In a compilation of strike-slip surface ruptures, Wesnousky (2006) reported that approximately half of the ruptures in the compilation end in an area that lacks a discontinuity, and the fault surface trace continues in the landscape. An analysis of fault sections that have at least two earthquakes in the historical record shows that spillover rupture of a few kilometers is common, even when the adjoining region has had a recent earthquake (Schwartz, 2018). Finally, precipitation and anthropogenic activity further complicate interpretation of the record created by each surface rupture because offset features are modified by geomorphic (e.g., Arrowsmith & Rhodes, 1994; Liu et al., 2004; Reitman et al., 2019; Salisbury et al., 2018) and anthropogenic (e.g., Lienkaemper & Strum, 1989) processes between earthquakes, and the precipitation rate of a region affects the distribution of offset channels preserved along a fault (Reitman et al., 2023).

Here, we investigate how characteristics of surface slip (along-strike slip variability, slip amplitude, slip distribution shape, and slip history) affect how slip-per-event and slip distribution are recorded in and interpreted from geomorphic data. We also investigate the assumptions and methods used to interpret offset measurement data sets to determine slip history, such as the effect that data density has on interpretation, whether density peaks record average slip for modern earthquakes, and how well non-characteristic slip can be interpreted with COPD methods. Finally, we examine the conditions required to preserve and interpret multiple generations of surface slip in geomorphic data. We do so by applying standardized COPD methods to (a) slip distribution data from 39 modern strike-slip surface ruptures, (b) offset measurement data from 29 strike-slip faults with geomorphic evidence of multiple earthquakes (cumulative offsets), and (c) synthetic strike-slip slip distributions with artificial noise. The results of this work will inform future interpretation of slip history from offset measurement data along strike-slip faults.

2. Background

2.1. Cumulative Offset Probability Distribution (COPD) History

The cumulative offset probability distribution (COPD) method is often used to interpret paleo-slip amplitude and distribution from offset geomorphic landforms along strike-slip faults (Figure 1). The COPD method was first used by McGill and Sieh (1991) to interpret paleo slip on the Garlock fault, used by Klinger et al. (2000) on the Dead Sea Fault, and named by Zielke et al. (2010) who applied it to the Carrizo section of the San Andreas Fault. These researchers noted that offset measurements cluster in size, and they interpreted those clusters to represent average slip in one or more past earthquakes, with the smallest measurements representing slip in the MRE if storms that form geomorphic markers happen more frequently than earthquakes (Grant Ludwig et al., 2010; Zielke et al., 2010). The method has been widely adopted since 2010, used in more than 20 studies (Table 1).

Early studies applied the COPD method in one dimension (1D COPD) (Klinger et al., 2011; McGill & Sieh, 1991; Zielke et al., 2010) to infer slip history from the peaks in the density function. The 1D COPD method is applied to an entire studied fault (e.g., Klinger et al., 2011; Ou et al., 2020) or for each interpreted fault section to honor independent slip histories of different fault sections (e.g., Ansberque et al., 2016; Benjelloun et al., 2021; Bi et al., 2020; Haddon et al., 2016; Jiang et al., 2017; Kang et al., 2020; Klinger et al., 2000; Kurtz et al., 2018; McGill & Sieh, 1991). The downside of 1D COPD analysis for interpreted fault sections is that endpoints of paleoseismic ruptures are often unknown and may not follow structural segment boundaries (e.g., Schwartz, 2018; Wesnousky, 2006). Additionally, interpreting average slip from peaks in a 1D COPD inherently

Table 1
Faults With Geomorphic Evidence of Multiple Earthquakes Compiled in Reitman et al. (2023) and Included in the Analysis

Data source	Fault (section)	COPD CV[a]	KDE CV[b]	Pub. CV[c]	Characteristic slip in publication?	Quote on characteristic slip from publication
Ansberque et al. (2016)	Longriqu	0.25	0.46	0.28	Yes	"The Longriqu fault zone follows a characteristic slip model with a 4̃ m coseismic slip"
Benjelloun et al. (2021)	Middle North Anatolian (eastern)	0.15	0.34	N/A	Possible	"Our data set remains compatible with a "characteristic slip" behavior, as in scenarios 1 and 2, where the earthquakes show recurring, similar slip distributions."
Bi et al. (2020)	West Henlanshan	0.58	0.38	0.35	Yes	"Large paleoearthquakes have produced characteristic slip along the fault with a lateral slip of 3̃ m and a vertical slip of 1̃ m"
De Pascale et al. (2014)	Alpine	0.25	0.21	0.25	Possible	"If explanation 1 is true, the Alpine fault has two (i.e., bimodal) or more modes of behavior […] If explanation 2 is true, perhaps the Alpine fault behavior is characteristic, and other faults are responsible for some shaking records. Ultimately, bimodal behavior is our preferred interpretation."
Elliott et al. (2015)	Altyn Tagh (Annanba)	0.51	0.31	N/A	Not discussed	Not discussed
Guo et al. (2019)	Lenglongling	0.45	0.46	N/A	Yes	"…indicating that the fault ruptures with a characteristic slip"
Haddon et al. (2016)	Owens Valley	0.43	0.22	0.30	Not discussed	Not discussed
N. Han et al. (2018)	Altyn Tagh (Xorkoli)	0.33	0.31	0.48	Not discussed	Not discussed
N. Han et al. (2018)	Altyn Tagh (Xorkoli-Annanba)	0.29	0.29	0.32	Not discussed	Not discussed
S. Han et al. (2019)	Burgar Co	0.47	0.47	0.51	Unlikely	"Therefore the most recent cumulative offsets process of the BGCF does not totally conform to the pattern of characteristic slip"
Jiang et al. (2017)	Yishu (F5)	0.04	0.27	0.05	Yes	"The YSFZ has followed a characteristic slip model during the Holocene"
Kang et al. (2020)	Altyn Tagh (eastern)	0.26	0.30	0.10	Yes	"The distribution of offsets and paleoseismological data reveal that the eastern Altyn Tagh fault exhibits characteristic slip behavior"
Klinger et al. (2011)	Fuyun	0.03	0.02	0.04	Yes	"We conclude that ruptures on the Fuyun fault obey a characteristic slip model"
Kurtz et al. (2018)	Bogd	0.57	0.81	N/A	Possible	"Cumulative offsets of geomorphic features suggest that the Eastern Bogd fault might produce characteristic slip over the last seismic cycles"
H. Li et al. (2012)	Karakax	0.36	0.35	0.24	Yes	"We interpret the other offset clusters as the possible repetition of similarly sized events thus favoring a characteristic slip model for the Karakax fault"
X. Li et al. (2017)	Tianjingshan (western)	0.35	0.35	0.15	Likely	"Measurements of 240 offset streams and ridges confirm that the fault is left-lateral and record evidence of repeated ∼3–4 m coseismic offsets along the 60–km–long fault. This suggests that ∼6 earthquakes may have occurred along the entire western Tianjingshan fault with repeated occurrence of earthquakes of Mw 7.2–7.5."
Lindvall et al. (1989)	Superstition Hills	0.24	0.22	N/A	Possible	"The test for a pre-1987 slip event identical to the 1987 event produces a strong concentration of residuals about the zero value, supporting the characteristic earthquake hypothesis for the penultimate event…The data are too sparse to conclusively test the characteristic earthquake hypothesis for any slip events earlier than the penultimate event."
Manighetti et al. (2015)	Hope (eastern)	0.60	0.47	0.42	Likely	"This supports the suggestion that large prehistorical earthquakes on the eastern Hope Fault might have produced a characteristic surface slip of 4.4 ± 1m at the site of study."
Manighetti et al. (2020)	Wairarapa	1.03	1.14	0.06	Likely	

Table 1
Continued

Data source	Fault (section)	COPD CV[a]	KDE CV[b]	Pub. CV[c]	Characteristic slip in publication?	Quote on characteristic slip from publication
						"Modeling the entire offset data set reveals 7 prior earthquakes ruptured the entire fault, each similarly producing 16.9 ± 1.4 m dextral slip and 0̃.6 m vertical slip"
McGill and Sieh (1991)	Garlock (central)	0.46	0.46	N/A	Not discussed	Not discussed
McGill and Sieh (1991)	Garlock (eastern)	0.53	0.31	N/A	Not discussed	Not discussed
Ou et al. (2020)	Haiyuan	0.55	0.57	N/A	Not discussed	Not discussed
Ren et al. (2016)	Haiyuan	0.77	0.79	N/A	Unlikely	"Therefore, the COPD clusters at multiples of 5 m cannot be simplified to represent the characteristic earthquake or uniform slip models."
Rizza et al. (2011)	Bogd	0.13	0.13	N/A	Yes	"This observation suggests that the cumulative displacements observed along the Bogd Fault are multiples of the 1957 offset, and is consistent with a characteristic slip distribution."
Salisbury et al. (2012)	San Jacinto (Clark)	0.41	0.50	N/A	Possible	"Thus, these geomorphic observations argue for semicharacteristic slip along the Clark fault."
Xiong and Li (2020)	Altyn Tagh (Xorkoli)	0.21	0.39	0.26	Yes	"Implying that the 11 successive event ruptures along the Altyn Tagh fault followed the characteristic slip pattern."
Zielke et al. (2010)	San Andreas (Carrizo Plain)	0.16	0.16	0.09	Possible	"Earthquake slip along the Carrizo segment may recur in earthquake clusters with cumulative slip of 5̃ meters."
Zielke et al. (2012)	San Andreas (1857 rupture)	0.44	0.45	N/A	Unlikely	"A tentative reconstruction of pre-1857 earthquake surface slip provides no evidence that supports the hypothesis of a characteristic recurrence of 1857-like earthquakes."
Zinke et al. (2021)	Wairau (central)	0.24	0.33	N/A	Not discussed	Not discussed

[a]Coefficient of variation (CV) of slip-per-event calculated from 1D cumulative offset probability distribution (COPD) peaks. [b]Coefficient of variation (CV) of slip-per-event calculated from 1D kernel density estimate (KDE) peaks. [c]Coefficient of variation (CV) of slip-per-event calculated from publication. "N/A" indicates not possible to calculate CVslip-per-event from publication.

assumes earthquakes have approximately constant slip along a fault or fault section and that average slip is represented by the modal measurement values. Later studies used two-dimensional COPD (2D COPD) analysis with spatial bins to interpret paleo-slip distributions along a fault without interpreting rupture endpoints explicitly (Bi et al., 2022; Chen et al., 2018; Haddon et al., 2016; Ren et al., 2016; Zielke et al., 2012), but most of the paleo-slip distributions interpreted from 2D COPD analysis are presented without uncertainty bounds (e.g., Bi et al., 2022; Chen et al., 2018; Haddon et al., 2016; Zielke et al., 2012). The 2D approach allows for along-strike slip variability, unknown rupture endpoints, and interpretation of independent slip histories on multiple fault sections along a fault.

2.2. Prior Work

Prior studies investigating how well the geomorphic record resolves evidence of strike-slip surface rupture have contrasting results, reporting that up to five (Zielke, 2018) or only two or three (Lin et al., 2020) earthquakes can be interpreted from 1D COPD peaks. Both studies analyzed 1D COPD curves to determine if the density peaks were representative of earthquake slip, with Zielke (2018) doing so with numerical models that simulate storms that create and destroy geomorphic markers and earthquakes that offset them and Lin et al. (2020) using offset measurement data from 35 modern surface ruptures modeled to simulate geomorphic offset markers that record multiple earthquakes.

There are a few key limitations with these studies. First, both studies use 1D analysis methods and focus on the recording potential of density peaks, but many researchers use 2D methods to interpret paleo-slip distribution along a fault (e.g., Bi et al., 2022; Chen et al., 2018; Haddon et al., 2016; Zielke et al., 2012). Second, both studies interpret limited randomly selected geomorphic markers; it has not been tested if the same methods applied to a many sets of random offset markers would have the same result. Third, the values of along-strike slip variability (10%–30%) and measurement uncertainty (5%–15%) are on the low end of the observed range for modern earthquakes in the Zielke (2018) study, and the conclusions are based on 10% measurement uncertainty and 20% slip variability. Analyzing data from a compilation of modern strike-slip surface ruptures, Lin et al. (2020) found average surface slip variability of 0.58–0.66, and Reitman, Mueller, and Tucker (2022) found average surface slip variability of 0.43–0.52. For measurement uncertainty, Zielke (2018) bases the 5%–15% range on a study that has a single user re-measure the same feature multiple times (P. O. Gold et al., 2013). Studies that have multiple users measure the same offset landform (Salisbury et al., 2015; Scharer et al., 2014) find larger uncertainty, ≥20%–30%, because interpretation uncertainty of an offset feature is commonly greater than measurement uncertainty (Salisbury et al., 2015; Scharer et al., 2014).

Our study builds on this prior work and addresses these limitations. First, we use 2D methods in addition to 1D because we investigate how well along-strike slip distributions can be recorded and interpreted. Second, we run multiple iterations of each numerical simulation to ensure that we do not base conclusions on one set of randomly selected data. Third, we use large ranges of surface slip variability (0%–100%) and slip-per-event (0–10 m) values to explore a broad parameter space that encompasses the majority of values observed in modern earthquakes. Additional distinctions from prior work are that we use three large data sets (modern strike-slip earthquakes, faults with geomorphic evidence of multiple earthquakes, and numerical simulations); investigate the effects of slip distribution shape and non-characteristic slip in addition to along-strike slip variability; and propose updated methods for interpreting paleo-slip distributions.

3. Data and Methods

3.1. Methods

Following established methods (e.g., Haddon et al., 2016; Klinger et al., 2011; McGill & Sieh, 1991; Zielke et al., 2012), we calculate cumulative offset probability distribution plots in one dimension (1D COPD) and in two dimensions with spatial bins (2D COPD). We also calculate kernel density estimates (KDEs) for each data set in 1D and 2D with Gaussian kernels. KDEs are a type of density estimate using a kernel to make an aggregate PDF of a data set. The KDE approach is not necessarily better than COPD for earthquake geology because a KDE does not take into account variable measurement uncertainty. We show the KDE plots because they are objective and require no user input and thus are useful as a quick, unbiased treatment of offset measurement data to augment COPD analysis. We analyze each data set with the same parameters and without user input. For each data set, we plot all offset measurements with reported uncertainty along the fault (Figure 1a), all offset measurements with uncertainty sorted from largest to smallest (Figure 1b), a 2D COPD with spatial bins determined by fault length (Figure 1c), a 1D COPD with peak heights identified with SciPy Signal's "find_peaks" algorithm (Virtanen et al., 2020) (Figure 1d), a 2D KDE with a bandwidth of 0.3 using Seaborn's "kdeplot" algorithm (Waskom, 2021) (Figure 1e), and a 1D KDE with a bandwidth of 0.15 using SciPy Stats' "gaussian_kde" (Virtanen et al., 2020) with peak heights identified automatically (Figure 1f). Bandwidth has a large effect on KDE outcome, and the bandwidths used here are selected to be similar to COPD results. We found that a 0.15 bandwidth for the 1D KDE best matched 1D COPD curves. We use a 0.3 bandwidth for the 2D KDE to facilitate interpolation along strike.

We take the following steps to construct each 2D COPD: (a) construct a PDF for each measurement based on the preferred, minimum, and maximum offset values; (b) choose the size of the spatial bins for the 2D approach; (c) sum the individual measurement PDFs in a bin (all measurements for the 1D approach) into an aggregate probability curve; and (d) normalize probability within each spatial bin.

Multiple decisions go into a COPD analysis in 1D or 2D. The first decision is how to construct PDFs for each offset measurement. We test four options: (a) a normal (Gaussian) distribution with the preferred offset value at the center and standard deviation based on preferred, minimum, and maximum offset; (b) a normal (Gaussian) distribution with the preferred offset value at the center and truncated at the minimum and maximum offset values ("truncnorm"), (c) a triangular distribution from the minimum to maximum offset values with a peak at the preferred offset value ("triangular"); and (d) a uniform distribution from the minimum to maximum offset values ("uniform") (Figures S1 and S2 in Supporting Information S1). Except where noted, all analysis is conducted using the non-truncated normal distribution. The normal distribution produces results most similar to published 1D COPD analyses and enables a broader uncertainty range than the other PDF construction methods. The

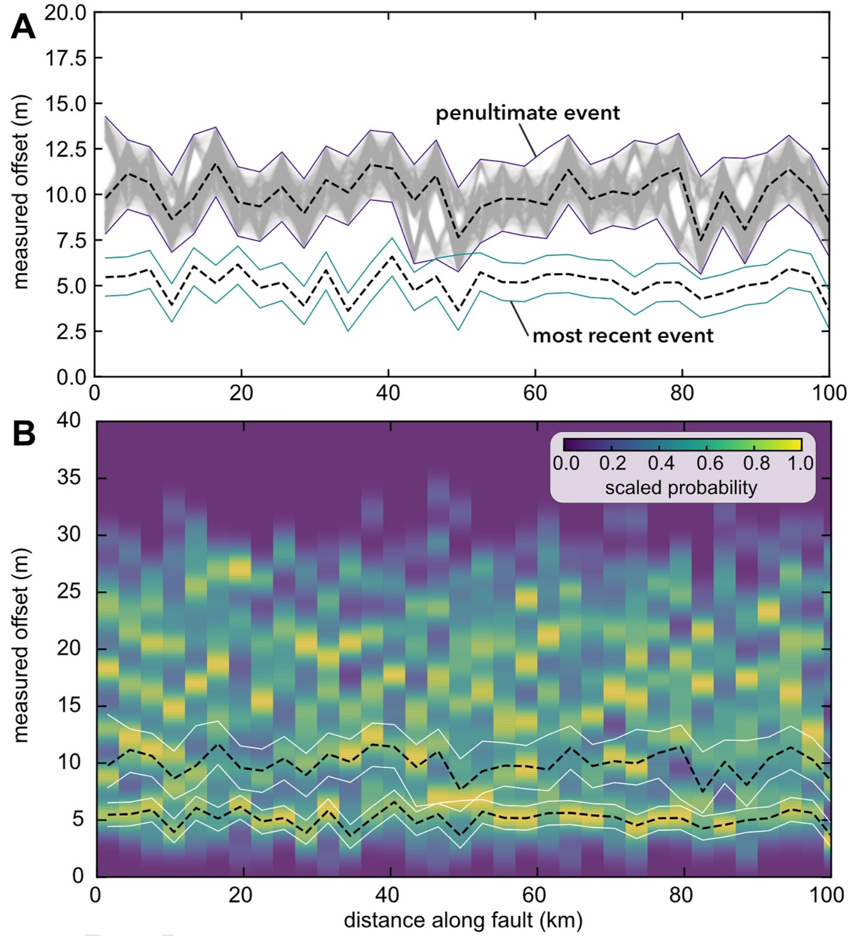

Figure 2. (a) Slip distributions interpreted from the most recent and penultimate earthquakes from a synthetic data set with five 5-m-slip earthquakes and 30% noise (same as in Figure 1). The set of possible slip distributions (gray lines) are constructed by randomly selecting from the values with the top 20% probability within each bin 1,000 times. Possible preferred slip distributions (dashed black lines) are shown as the median of each bin. Uncertainty (purple and teal lines) are minimum and maximum of each bin. Light gray lines show 1,000 possible slip distributions. (b) The slip distributions calculated from each event imposed on the two-dimensional cumulative offset probability distribution (2D COPD) calculated from the full data set, as in Figure 1C.

broader uncertainty range from the normal distribution is most representative of true uncertainty because geomorphic offset data have been affected by an unknown amount of geomorphic change over multiple earthquake cycles. The truncnorm, triangular, and uniform PDF methods result in COPDs with more peaks, but the overall signal is similar for all four methods (Figure S2 in Supporting Information S1).

The second decision is the size of the spatial bins in the 2D COPD approach. After testing various numbers and sizes of bins, we use a default value of 1/30th of fault length, rounded down to the nearest whole kilometer, with 0.5-km bins for ruptures <30-km long. We choose a dynamic bin size because data density tends to scale inversely with studied fault length (calculated from the data in Table 1 in Reitman, Mueller, & Tucker, 2022), so long faults with small bins would have many bins without data. The third decision is whether and how to normalize aggregate probability, with options to do so within each bin, within each peak, or across the entire data set. The 2D KDEs in our analysis are normalized across the data set, and the 2D COPDs are normalized within each bin. Both 1D methods are normalized for the single curve. Finally, some may choose to weight individual PDFs by quality in summing them into a COPD, but we believe that the quality of a measurement is captured by the range of minimum to maximum offset values.

10.1029/2024JB028692

3.2. Slip Distributions

The final step is to construct a set of possible slip distributions from the 2D COPD (Figure 2). We construct the set of possible slip distributions by randomly selecting values from the top 20% probability within each peak in each bin 1,000 times, and connecting ruptures along the fault into slip distributions. Sampling can be weighted by probability or based on uniform chance across each peak range. We used the top 20% probability in each peak because 20% is a typical value for offset marker uncertainty (e.g., Salisbury et al., 2015; Scharer et al., 2014). We do not apply other filters in constructing the set of possible slip distributions. The slip distributions could optionally be filtered based on site-specific data (e.g., trench results or a suite of dated terraces), average/maximum displacement scaling relationships, displacement-length scaling relationships, slip variability, or compliance with the elastic strain limit (although slip gradients in recent ruptures do not always obey the elastic strain limit e.g., C. Li et al., 2023). This approach results in a large set of possible slip distributions that define uncertainty bounds (solid lines in Figure 2) on the interpreted preferred slip distribution.

3.3. Data

We apply the above methods to analyze offset measurements data sets from 39 modern (i.e., recent and historical) strike-slip surface ruptures compiled in Reitman, Mueller, and Tucker (2022) (Figure 3, Table S1 in Supporting Information S1), offset measurements on 29 faults with geomorphic evidence of multiple earthquakes compiled in Reitman, Klinger, et al. (2022) (Figure 4, Table 1), and synthetic slip distributions with artificial noise constructed for this study (e.g., Figure 1). For modern surface ruptures, we exclude data sets with <15 measurements. From the geomorphic offset measurement data sets, we exclude data sets that are primarily one earthquake or include creep. This results in a set of COPD and KDE peak values for each modern and geomorphic data set analyzed following a standard 1D approach and a visual representation of 2D cumulative probability. For the faults with geomorphic evidence of multiple earthquakes, we also compiled or calculated the coefficient of variation (standard deviation/mean) of slip-per-event ($CV_{slip-per-event}$) from COPD peak values in the papers that reported the information ($n = 16$ of 29).

To make synthetic slip distributions, we construct flat and elliptical distributions with 1–10 m average slip for the flat distribution and 1–10 m maximum slip for the elliptical distribution and add 0%–100% random noise (Figures 5, S3 in Supporting Information S1). We chose flat distributions because they are the simplest test and provide a best case scenario result. We additionally model elliptical distributions because they provide somewhat more realistic slip distribution based on modern ruptures (e.g., Wesnousky, 2008). We use 1–10 m average slip to simulate most of the range of observed offsets in modern ruptures and use 0%–100% random noise (normally distributed) to cover the full range of possible along-strike variability. To simulate multiple earthquakes, we propagate the slip distributions five times, with random noise added to the prior data points for each earthquake (Figures 6, S4 in Supporting Information S1). We use random noise to simulate the variability introduced by three processes: (a) on-fault surface slip variability that can vary within short spatial scales along a surface rupture (e.g., R. D. Gold et al., 2015; Haeussler et al., 2004; McGill & Sieh, 1991; Rockwell & Klinger, 2013), (b) interpretation uncertainty and measurement error of cumulative offsets (Salisbury et al., 2015; Scharer et al., 2014), and (c) geomorphic change of offset markers after an earthquake or during the interseismic period (Arrowsmith & Rhodes, 1994; Liu et al., 2004; Reitman et al., 2019; Salisbury et al., 2018).

To enhance the robustness of this approach and to avoid over-interpreting a single set of random synthetic slip distributions, we test all combinations of 1–10 m of slip and 0%–100% noise with 1-m and 10% increments. For each combination of slip and noise, we make 100 flat slip distributions with five earthquakes based on different random seeds, for a total of 11,000 flat synthetic slip distributions. For each iteration, we calculate the coefficient of variation of slip-per-event ($CV_{slip-per-event}$, standard deviation/mean) from 1D COPD and KDE peak values and the normalized root mean squared error (nRMSE) of COPD peak values. We calculate nRMSE by comparing the slip value at peak density to the imposed slip amount and normalizing by imposed slip to account for the large range in slip values. We average $CV_{slip-per-event}$ and nRMSE for all 100 iterations of each combination of slip and noise (Figure S5 in Supporting Information S1).

10.1029/2024JB028692

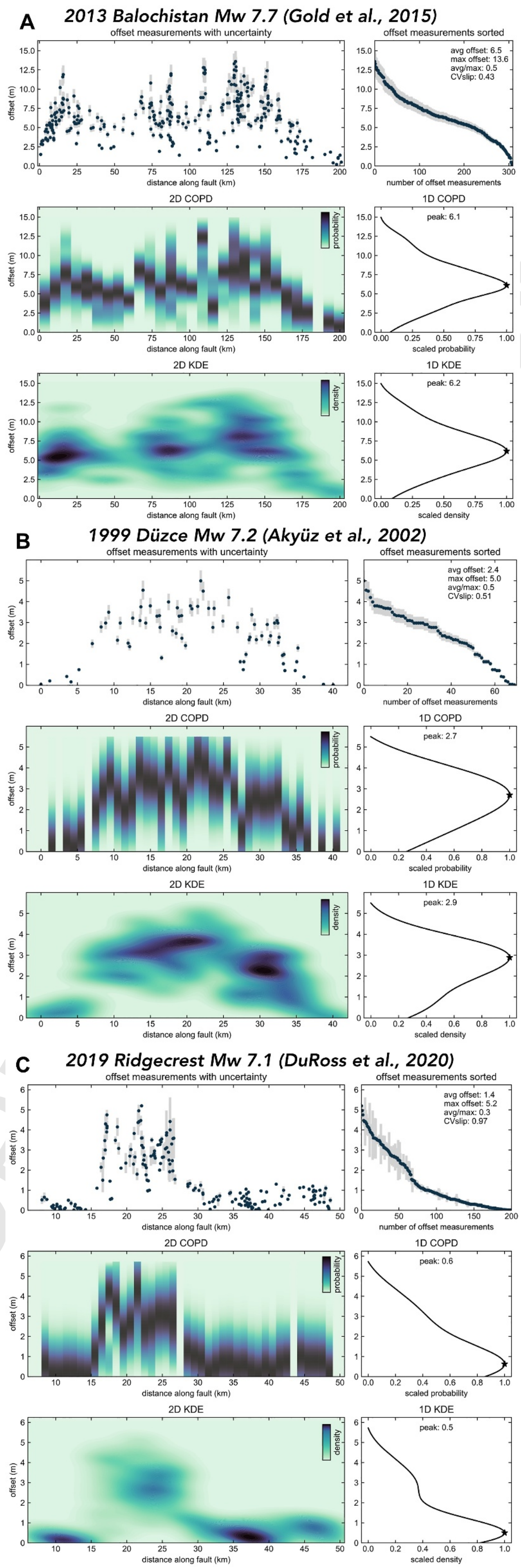

Figure 3. The cumulative offset probability distribution (COPD) and kernel density estimate (KDE) methods applied to three examples of recent ruptures with offset data measured by hand. (a) Balochistan 2013 near field data (R. D. Gold et al., 2015), (b) Düzce 1999 (Akyüz et al., 2002), and (c) Ridgecrest 2019 Mw7.1 (DuRoss et al., 2020). Refer to Figure 1 for a detailed explanation of each sub-panel and the supplemental material for plots of all single-earthquake data sets. CVslip: Coefficient of variation of slip along strike.

4. Results

4.1. Insight From Modern Slip Distributions

With modern strike-slip surface ruptures we test some of the assumptions in the COPD method and investigate how known surface ruptures would be interpreted from COPD methods (Figure 3). From the set of 39 modern surface ruptures, we compare modal offset values (the highest peak in a 1D COPD or KDE) to a simple average slip taken as the mean of all measurements (not accounting for data density) and to average slip as reported by the authors of the study (Figure 7). We assume that most authors calculate the reported mean slip more carefully than a simple average of all data. We find that slip amounts interpreted from COPD and KDE modal offset values are not significantly different (paired t-test, $p = 0.10$) and are strongly correlated to both simple and reported average slip, with a Pearson correlation coefficient (r) of >0.91 for all comparisons ($p \approx 0.00$). Refer to supplemental material for plots of all data sets. Despite the strong correlation, the COPD and KDE peak values tend to underestimate both simple and reported mean slip because the modes of offset data differ from the means, and these differences are significant for all comparisons (paired t-test, $p < 0.05$). Although there are some outliers, this analysis supports the assumption that average slip in past earthquakes can be interpreted from 1D COPD or KDE peaks.

Next, we evaluate how variability of surface slip in modern ruptures is represented in 1D and 2D COPD approaches. Modern strike-slip surface ruptures measured by hand have average spatial variability within a fault or fault section ($CV_{slip-along-strike}$) of 0.43 (single section) to 0.50 (multiple section), with a large total range of 0.14–1.14 (Reitman, Mueller, & Tucker, 2022). Example surface ruptures with typical and high variability demonstrate what these ruptures look like in probability space (Figure 3). The 2013 Balochistan, Pakistan, earthquake has average slip variability, and 1D COPD and KDE peaks slightly underestimate simple average offset (Figure 3a). The 1999 Düzce, Turkey, earthquake has average slip variability, and 1D COPD and KDE peaks slightly overestimate simple average slip (Figure 3b). The 2019 Mw7.1 Ridgecrest, California, USA, earthquake has greater than average slip variability and the 1D COPD and KDE peaks greatly underestimate simple average slip (Figure 3c). Furthermore, the Ridgecrest Mw7.1 earthquake ruptured multiple fault sections with different slip distributions, and could be interpreted from the geomorphic record as two events because the 1D curve is bimodal with peaks at ~0.5 and 3 m. Approximately 20% of the modern surface ruptures we analyzed have a bimodal curve in 1D COPD or KDE analysis. Although it is possible to consider rupture geometry for modern earthquakes to apply COPD interpretation for individual fault sections, that information is usually not available for geomorphic data sets.

Finally, distributed deformation ~100–1,000 m from the primary fault trace has been observed in modern surface ruptures, accommodating 15% to >50% of the total deformation (Antoine et al., 2021; R. D. Gold et al., 2015, 2021; Milliner et al., 2015; Rockwell et al., 2002; Vallage et al., 2015). Distributed deformation is unlikely to be preserved in the geomorphic record because small cracks and offsets heal quickly in precipitation events following earthquakes. Thus, COPD analyses will likely underestimate slip in areas of substantial distributed deformation and act as a lower bound on fault slip.

4.2. Insight From Paleo-Slip Distributions

From re-evaluation of 29 data sets, we find mean and distribution of $CV_{slip-per-event}$ from 1D COPD peaks is 0.39 ± 0.21 (1σ) (Table 1 and refer to supplemental material for plots of all data sets). From 1D KDE peaks, we find mean $CV_{slip-per-event}$ of 0.41 ± 0.22 (1σ), and the KDE and COPD $CV_{slip-per-event}$ means are not significantly different (paired t-test, $p = 0.35$) (Figure 8a). Of studies that reported peak heights such that we could calculate inferred slip in each event ($n = 16$), we find mean $CV_{slip-per-event}$ of 0.24 ± 0.16 (1σ). Considering only the 16 data sets for which we can calculate reported $CV_{slip-per-event}$, the difference between the mean COPD or KDE and reported $CV_{slip-per-event}$ values is not significant at the 95% confidence level (paired t-test, $p = 0.11$ for both COPD and KDE) (Figure 8b). Despite the insignificant differences between the means of the calculated and reported $CV_{slip-per-event}$ values, the distribution skews lower for the reported $CV_{slip-per-event}$ values than those calculated in this study (Figures 8a and 8b).

10.1029/2024JB028692

Most studies use 1D COPD curves to analyze data sets of offset markers, with the peaks in the curve interpreted to represent amounts of average slip in past earthquakes for a fault or single fault section. When these data sets are plotted in 2D COPD space, it is evident that 1D COPD treatment oversimplifies variability along strike (Figure 4). The 2D COPD approach also allows for independent slip histories on different fault sections without explicitly interpreting the locations of fault section boundaries. All of the data can be analyzed together, and any differences in slip accumulation on fault sections should be visible in the 2D analysis. The 2D COPD approach with spatial binning also reduces potential bias from varying data density along a fault (e.g., Figure 4a). For example, km ≈1–2 in Figure 4a has higher measurement density than any other spatial bin, but the 2D COPD ensures equal sampling along the fault. The 2D COPD also better highlights low data density. For example, in Figure 4b, the low data density in ≈50–60 m slip makes multiple peaks in the 1D COPD, but it is evident in the 2D COPD how few measurements correspond to those 1D peaks.

The studies that have incorporated 2D analysis often use the 2D COPD to interpret slip distributions in multiple earthquakes along the fault. However, these interpretations typically lack uncertainty bounds on the preferred slip distributions, and different analysis methods can result in different interpretations. Small analytical decisions, such as the bounds and scaling factor (standard deviation) used in each measurement PDF in COPD methods and the bandwidth (smoothing factor) used in KDE methods, have a large effect on resulting 1D peaks and if distributions in neighboring bins overlap in 2D methods.

4.3. Insight From Synthetic Slip Distributions

To evaluate the influence of slip variability, data density, slip distribution shape, slip amplitude, and a history of variable slip amplitude (i.e., non-characteristic slip) on cumulative probability and interpreted slip history, we analyze flat and elliptical synthetic slip distributions with artificial noise (a proxy for integrated slip variability, measurement uncertainty, and offset feature modification) that simulate one and five earthquakes (Figures 5 and 6, S3, S4 in Supporting Information S1).

4.3.1. Slip Variability (Noise)

We used the synthetic slip distributions with 0%–50% artificial noise for a single rupture to determine the effect that along-strike slip variability (noise) has on the shape of 1D COPD peaks and how well they record imposed slip (Figures 9a and 9b). For both flat and elliptical slip distributions, we found that increased variability creates broader peaks, but high noise levels can make bimodal distributions with two peaks. For the flat slip distributions, modal offset value ranges from 4.9 to 5.5 m for 0%–40% noise (imposed slip of 5 m plus noise), but the 50% noise data set has a bimodal distribution with peaks at 3.1 and 5.8 m. Results are similar for the elliptical slip distributions. Modal offset value ranges from 3.9 to 4.8 m for the 0%–40% noise data sets, and the 50% noise data set has a bimodal distribution with peaks at 1.6 and 4.3 m. These bimodal distributions could be incorrectly interpreted to represent two earthquakes.

4.3.2. Data Density

Using the same synthetic slip distribution shapes for one rupture with 0%–50% noise, we randomly sampled the data set to determine how many observations are needed to define 1D COPD peaks that reflect imposed slip when the measurements are not spatially correlated (Figures 9c and 9d). We find that at 30% noise, about 40–50 measurements are needed to get a representative peak height for a flat distribution when sampled randomly. For elliptical distributions, 50–60 measurements are needed at the 30% noise level. For both distribution shapes, small sample sizes ($n = 5$–10) are more likely to create curves with a bimodal distribution. Although there are fewer data points, the peak half-widths are narrower because there is more than one peak. Sparse data thus result in artificially low estimates of uncertainty because more defined peaks are created, when true uncertainty is higher because there are fewer data points.

4.3.3. Slip Distribution Shape

Synthetic slip distributions constructed to approximate geomorphic data for five 5-m-slip earthquakes illustrate the inherent difficulties in interpreting paleo-slip distribution. For one set of example flat slip distributions

10.1029/2024JB028692

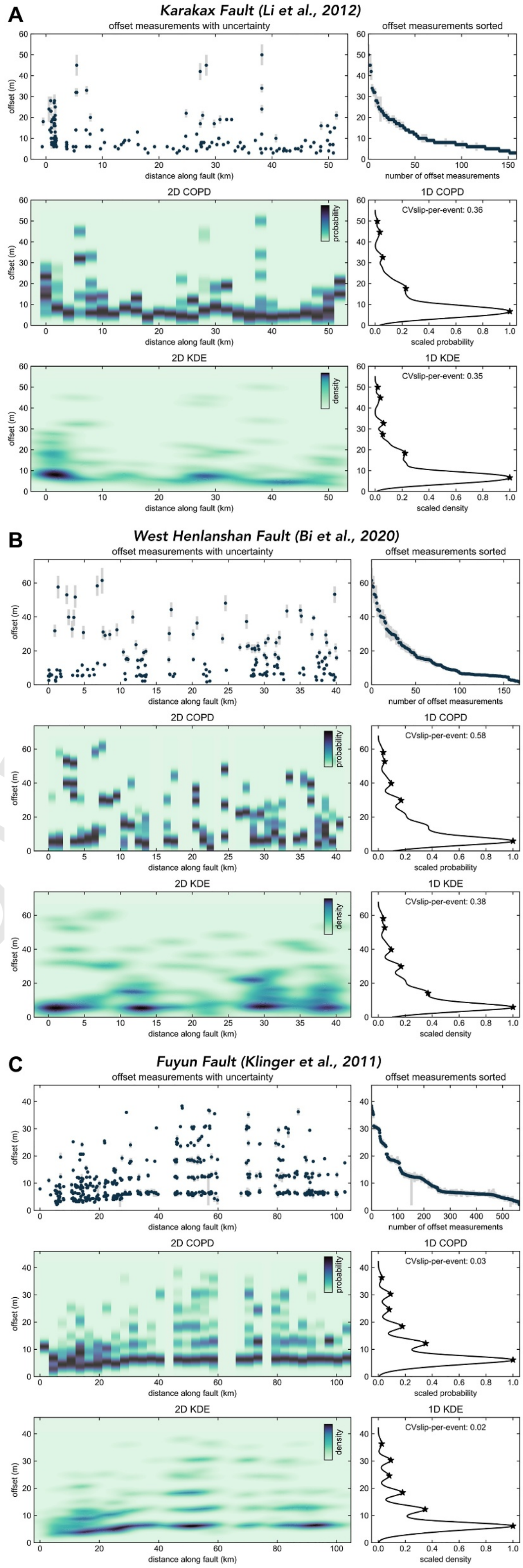

Figure 4. Examples of the cumulative offset probability distribution (COPD) and kernel density estimate (KDE) methods applied to geomorphic data sets. (a) The Karakax fault (H. Li et al., 2012), (b) the West Henlanshan fault (Bi et al., 2022), and (c) the Fuyun fault (Klinger et al., 2011). Refer to Figure 1 for a detailed explanation of each sub-panel and the supplemental material for plots of all geomorphic data sets. CVslip: Coefficient of variation of slip along strike.

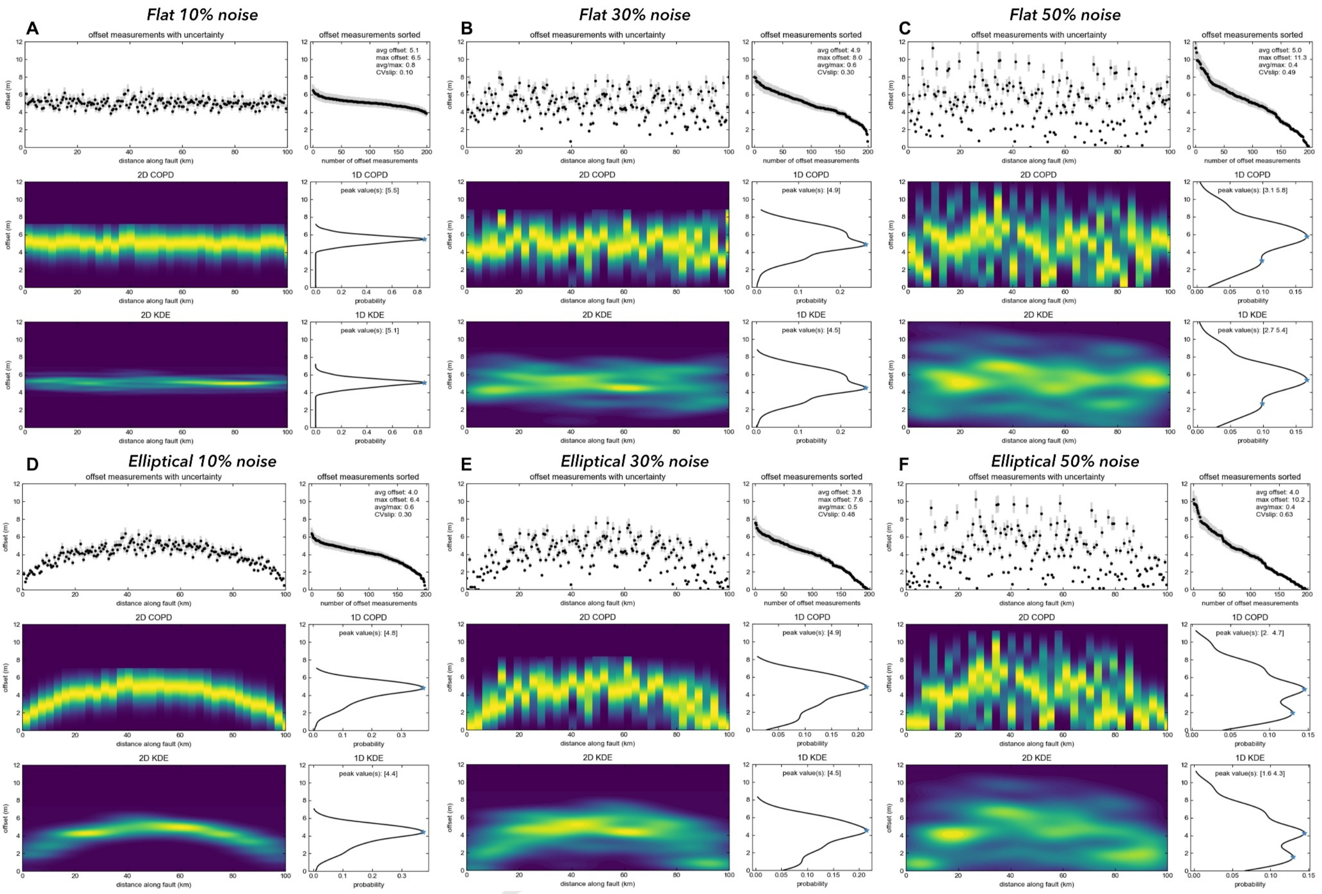

Figure 5. Simulated flat (a–c) and elliptical (d–f) slip distributions for one 5-m-slip earthquake with 10%, 30%, and 50% noise. KDE: kernel density estimate; COPD: cumulative offset probability distribution; CVslip: coefficient of variation of slip along strike.

(Figures 6a–6c, S4A–S4C in Supporting Information S1), 1D COPD peak values and slip distributions reflect the imposed slip history for 0%–10% noise (Figures 6a, S4A in Supporting Information S1). With 20% noise (Figure S4B in Supporting Information S1), offsets from different events begin to have overlapping slip values, the peaks in the 1D COPD approximate imposed average slip, and slip distributions can be distinguished for the first two earthquakes. With 30% noise (Figure 6b), the 1D peak values reflect imposed slip history, but only the most recent slip distribution can be reconstructed from the flat distributions. With 40%–50% noise (Figures 6c, S4C in Supporting Information S1), it is difficult to interpret the most recent slip distribution, and the 1D COPD peaks do not reflect the imposed 5-m-slip earthquakes.

For one set of example elliptical slip distributions (Figures 6d–6f, S4D–S4F in Supporting Information S1), 1D COPD peak values and slip distributions reflect the imposed slip history for 0%–10% noise (Figures 6d, S4D in Supporting Information S1). However, even with no noise, offsets from different events have overlapping slip values due to the elliptical shape of the distribution. With 20% noise (Figure S4E in Supporting Information S1), the lowest three 1D COPD peaks accurately reflect offset amounts, and slip distributions for the most recent and penultimate events can be reconstructed. With 30% noise (Figure 6e), the lowest three or four 1D peak values are similar to the imposed slip value, but only the most recent event slip distribution can be reconstructed for the elliptical slip distribution. With 40% noise (Figure S4F in Supporting Information S1), the lowest two 1D COPD peaks reflect imposed slip, and the most recent event slip distribution may be reconstructed. With 50% noise (Figure 6f), not even the most recent event slip distribution can be reconstructed with confidence, and the 1D COPD peaks do not reflect the imposed slip history. These results indicate that 1D COPD or KDE peaks do reasonably well capturing mean slip in past earthquakes for this permutation of random noise when noise is

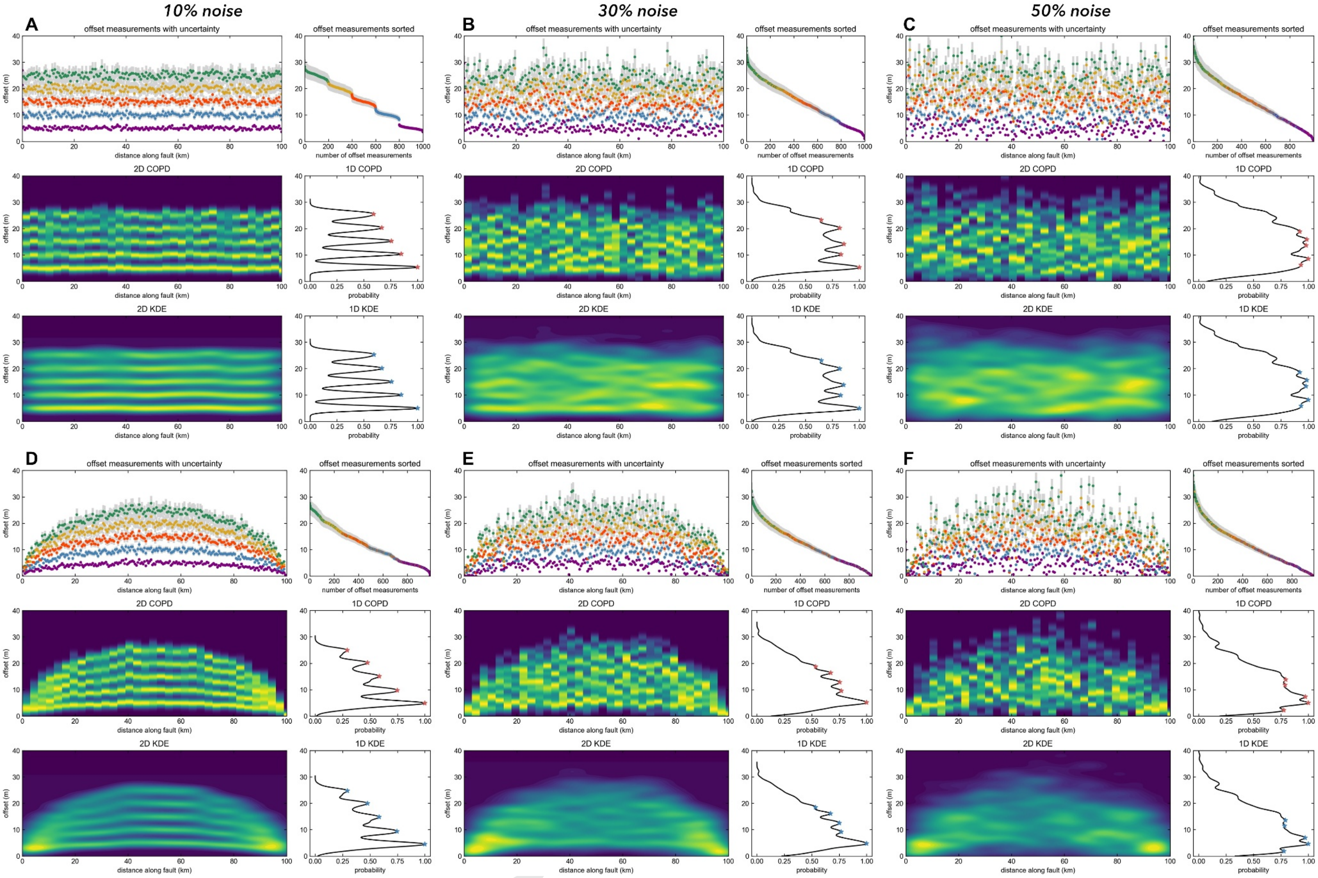

Figure 6. Simulated flat (a–c) and elliptical (d–f) slip distributions for five 5-m-slip earthquakes with 10%, 30%, and 50% noise. KDE: kernel density estimate; COPD: cumulative offset probability distribution; CVslip: coefficient of variation of slip along strike.

<50%, but it is difficult to interpret slip history for the penultimate and most recent earthquakes from the 2D COPD or KDE when noise is >30% for this permutation of random offset data.

These results indicate that with a flat or elliptical slip distribution, only two paleo-slip distributions can be distinguished with 20% noise, and only one with 30% noise, although average slip is recorded in 1D density peaks

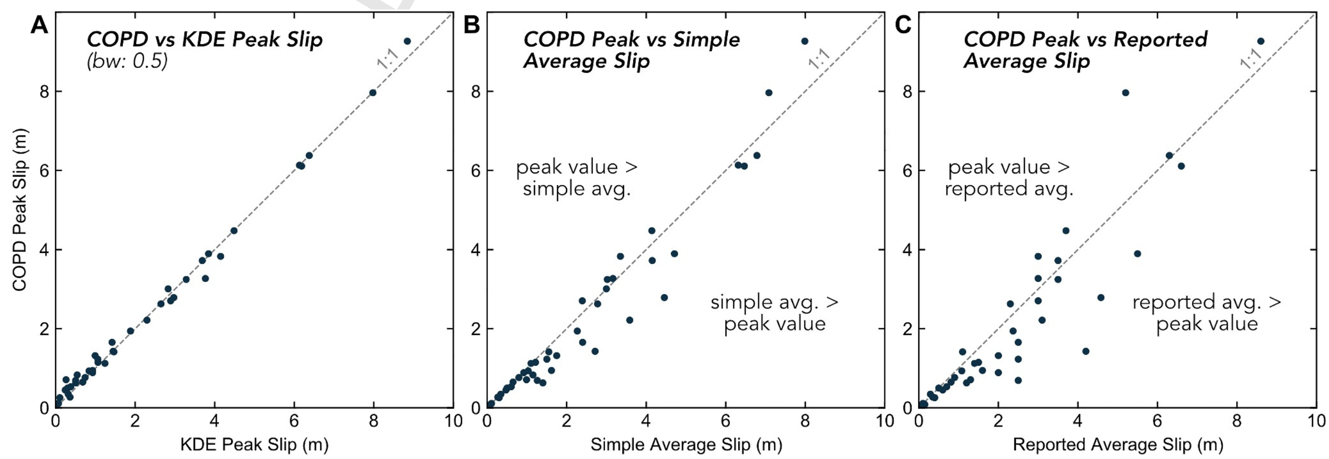

Figure 7. Comparison of average and modal (cumulative offset probability distribution (COPD) or kernel density estimate (KDE) peak) slip for 39 recent strike-slip surface ruptures. (a) Peak slip values from 1D COPD and KDE analysis. (b) COPD peak slip versus simple average slip. (c) COPD peak slip versus average slip reported by the authors of each study.

10.1029/2024JB028692

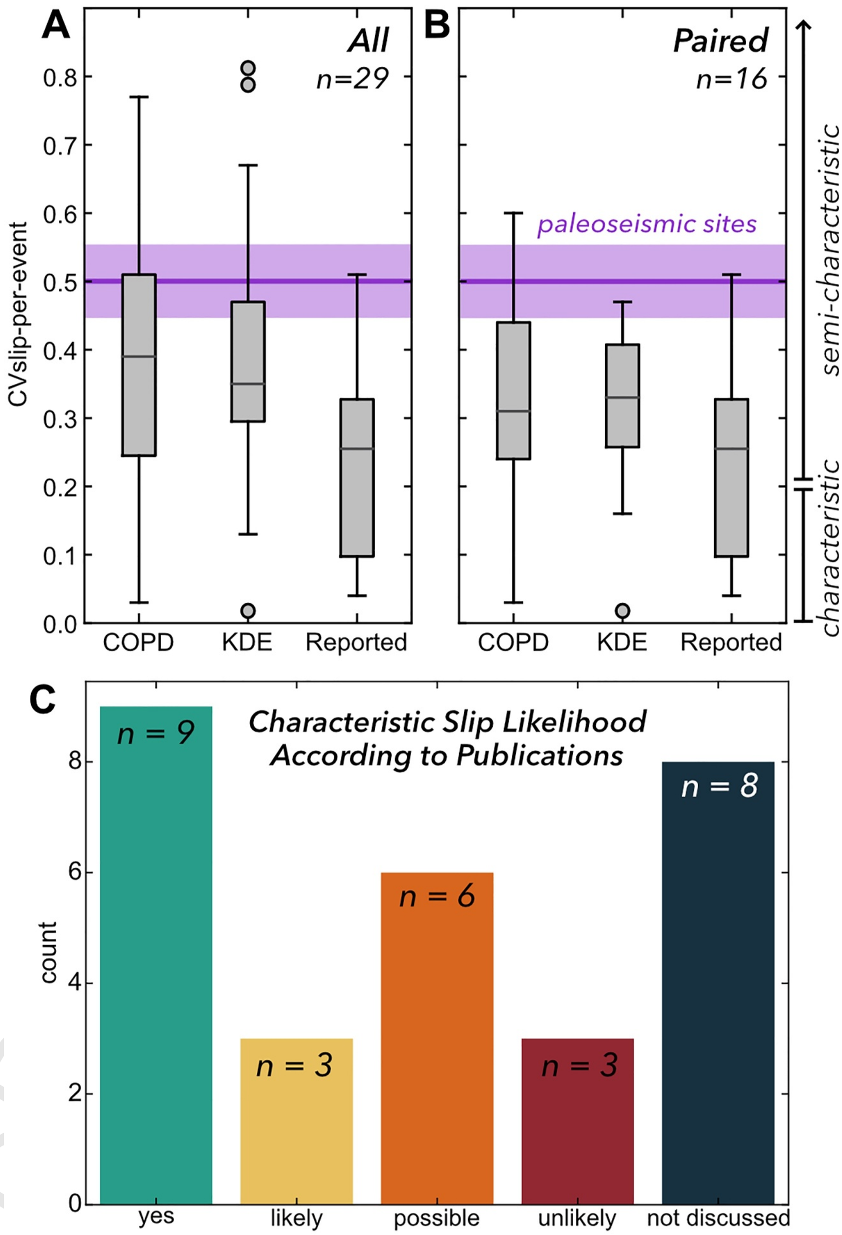

Figure 8. Coefficient of variation (CV) of slip-per-event data interpreted from analysis of offset geomorphic features. Cumulative offset probability distribution (COPD) and kernel density estimate (KDE) values are calculated from peaks in the 1D curves constructed for this study. Reported data are calculated from published peak values or COPD analyses. (a) All fault sections. (b) Only fault sections with reported values. Purple is CVslip-per-event range for paleoseismic sites from Hecker et al. (2013). (c) Likelihood of characteristic slip according to the original publications for the 29 data sets considered.

with 30% noise. However, these figures and interpretations depict one set of random synthetic offset data. For a more robust analysis, in the following section we consider a suite of synthetic data to test what can be determined at each noise level with varying slip amounts.

4.3.4. Characteristic Slip Amplitude and Noise

To test for an optimal combination of noise and slip amplitude that allows for robust peak interpretations that reflect slip history, we used 100 synthetic flat slip distributions for each combination of 0%–100% noise and 1–10 m slip (Figure 10). We show the mean $CV_{slip-per-event}$ and nRMSE of COPD peaks for all 100 iterations for each combination in Figure 10c and individual examples in Figures 10a, 10b, 10d, and 10e. Noise has a greater

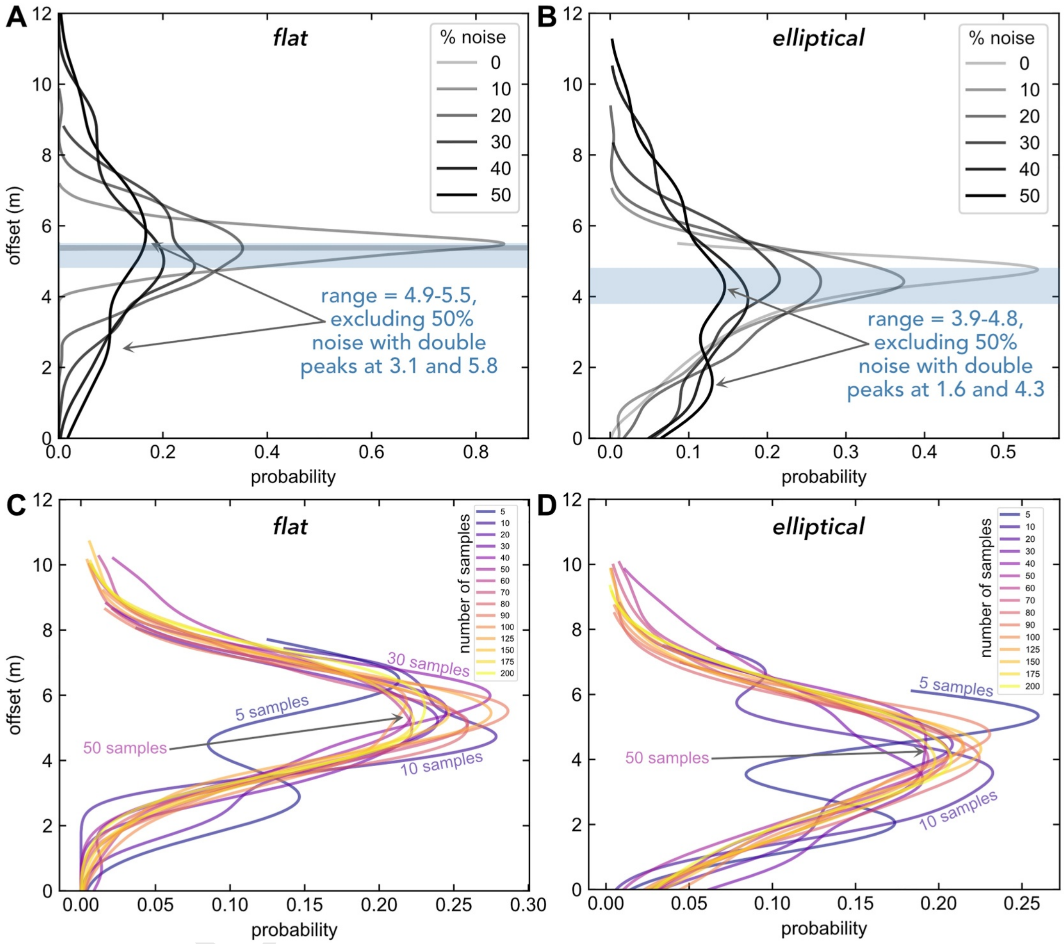

Figure 9. Examples of (a, b) slip variability's and (c, d) data density's effect on modal offset values (cumulative offset probability distribution (COPD) peak values) for one noise permutation for (a, c) flat and (b, d) elliptical synthetic slip distributions. Distributions in panels (c, d) have 30% noise.

effect on nRMSE than slip, with larger amounts of noise increasing nRMSE, until 40% noise. Average nRMSE has a threshold cutoff between 30% and 40% noise, where average nRMSE for data sets with ≥40% noise is the same regardless of slip amplitude and noise level. This analysis indicates that 1D COPD peaks for data sets with ≥40% variability do not robustly record average slip, regardless of slip amplitude, and 1D COPD analysis does reasonably well capturing average slip when noise is ≤30%. This result implies that 1D analyses may not correctly identify amounts of slip in paleo-ruptures for faults with along-strike slip variability of ≥40%, regardless of earthquake size.

4.3.5. Non-Characteristic Slip Amplitude and Noise

Finally, we test the effect of non-characteristic slip by mixing earthquakes with smaller and larger average slip and flat slip distributions to determine if the information can be interpreted from COPD methods. To test this, we construct flat synthetic slip distributions with five earthquakes alternating between large and small slip with large slip of 10 m and small slip ranging from 1 to 10 m (10%–100% of large slip), noise of 0%–100%, and 100 random iterations of each combination of small/large slip and noise (Figure 11). We find that when smaller earthquakes follow larger ones, small slip is more likely to be recorded in 1D COPD peaks if it is more than half the slip amplitude of the larger earthquakes (Figure 11a). With<20% noise, 1D COPD peaks will reflect imposed slip except when smaller slip is <10%–30% of large slip. With ≥20% noise, smaller slip must be at least 50% of larger slip to be recorded in 1D COPD peaks (Figure 11).

10.1029/2024JB028692

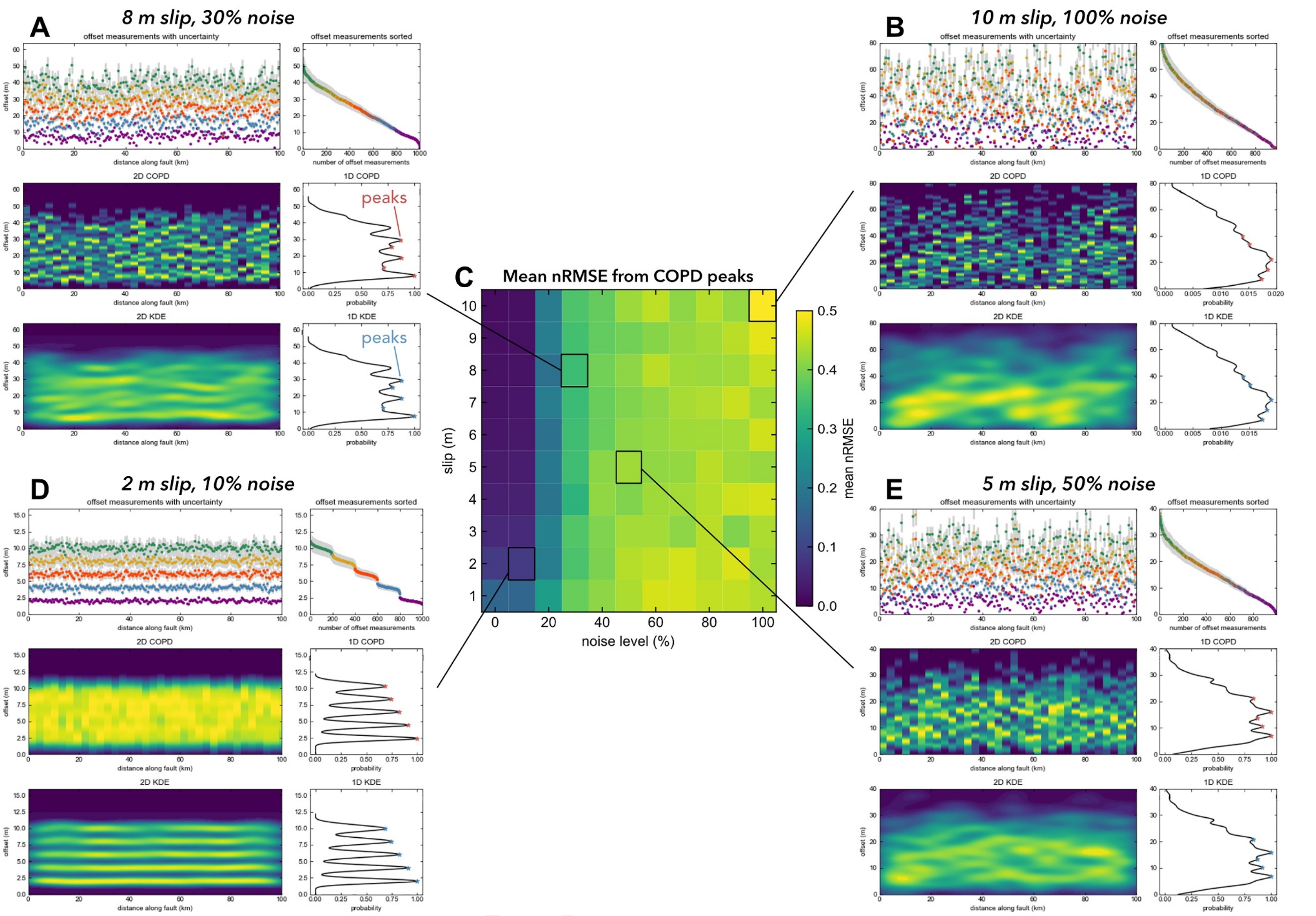

Figure 10. Synthetic characteristic slip distributions with different combinations of slip amplitude and noise (a, b, d, e) illustrate that 1D cumulative offset probability distribution (COPD) peaks (stars) for data sets with ≥40% variability do not robustly record average slip, regardless of slip amplitude. (c) Each box is the mean normalized root mean square error (nRMSE) from 100 random iterations of that combination of noise and slip. nRMSE is calculated by comparing slip-per-event values calculated from 1D COPD peaks to the amount of slip imposed in the model. KDE: kernel density estimate; CVslip-per-event: coefficient of variation of slip-per-event calculated from peak values.

5. Discussion

5.1. Implications for Interpreting Slip History

The results indicate that when noise in geomorphic offset measurements is >30%, it is difficult to reconstruct more than two slip distributions from offset geomorphic features and more than one with high confidence. Noise in geomorphic offset measurements is >30% for most faults due to surface slip variability that is inherent to the rupture process (e.g., Lin et al., 2020; Reitman, Mueller, & Tucker, 2022), the unpredictability of surface rupture end points (Schwartz, 2018; Wesnousky, 2006), the elliptical or other non-flat distribution of slip in most surface ruptures (Wesnousky, 2008), and variability that stems from manual interpretation and measurement of geomorphic features (Salisbury et al., 2015; Scharer et al., 2014). Geomorphic change between earthquakes compounds interpretation and measurement uncertainty by altering the landscape and offset features and increasing the potential variability between offset measurements (Reitman et al., 2019).

Although paleo-slip distribution is difficult to interpret in most cases beyond the MRE, peaks in the 1D COPD analysis may identify average slip in past earthquakes when noise is ≤30% and there are at least 40–50 offset measurements per event. These results agree with Lin et al. (2020), who found that only two or three earthquakes are recorded in 1D COPD peaks when surface slip variability is 25%–35%. Although the conclusions of Zielke (2018) are based on lower slip variability and measurement uncertainty values, their results for 30% slip variability and 15% measurement uncertainty also find that only three COPD peaks can be interpreted (Figure 5 in

10.1029/2024JB028692

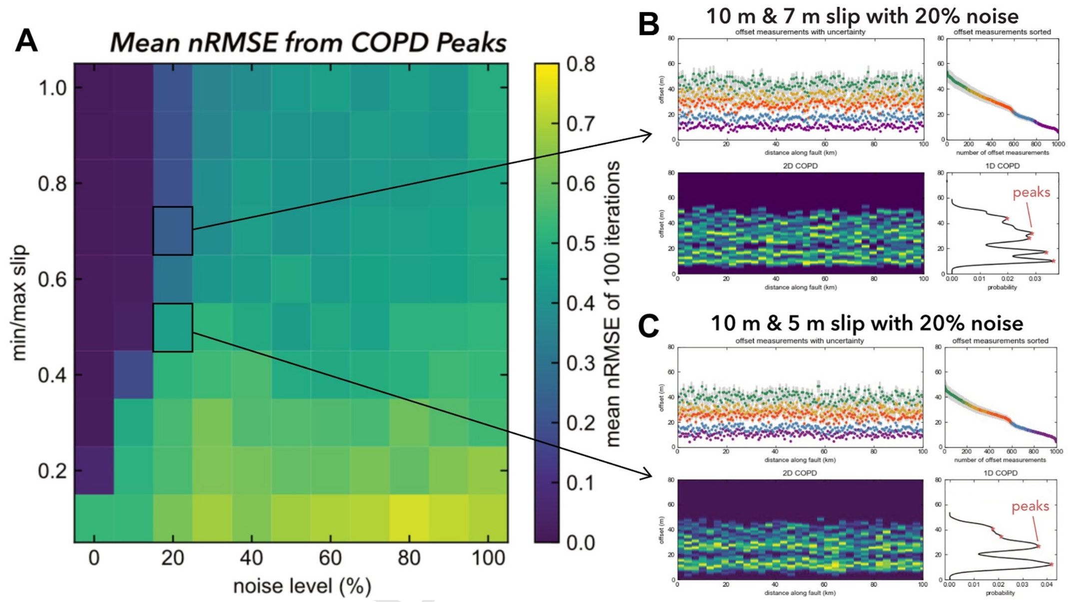

Figure 11. Testing non-characteristic slip with flat synthetic slip distributions. (a) Each box is the mean normalized root mean square error (nRMSE) for 100 iterations of that combination of small/large slip and noise. nRMSE is calculated by comparing slip-per-event values calculated from 1D cumulative offset probability distribution (COPD) peaks (stars) to the amount of slip imposed in the model. (b) One example of 10-m and 7-m slip earthquakes with 20% noise. (c) One example of 10-m and 5-m slip earthquakes with 20% noise. CVslip-per-event: coefficient of variation of slip-per-event calculated from peak values.

Zielke, 2018). Thus, three studies with three different approaches all find that only 2–3 1D COPD peaks can be interpreted from geomorphic offset measurements with typical slip variability.

These difficulties highlight the need for uncertainty bounds on interpreted paleo-slip distributions to assess the robustness of interpreted paleo slip. Using the method described in Section 3.2, we construct slip distributions and uncertainty bounds from synthetic offset measurements known to be from the most recent and penultimate earthquakes (purple and blue circles in Figure 1a) separately for a data set with 30% noise and five 5-m-slip earthquakes, a best case scenario. We then overlay these slip distributions on the 2D COPD from the full data set (Figure 2b). The MRE slip distribution corresponds well with high probability regions in each bin of the 2D COPD, but the penultimate event slip distribution correlates with high probability regions in some bins and is mismatched in others. The uncertainty bounds help capture the slip distribution range, but these slip distributions constructed for each earthquake individually are different from those that would be interpreted from analysis of the full data set all together. This exercise underscores the limitations in interpreting paleo-slip distributions from 2D COPD analysis and importance of reporting uncertainty bounds on interpreted paleo-slip distributions.

A fundamental limitation of 1D probability density methods is the potential for different slip histories on neighboring fault sections. This limitation is illustrated by studies that find different 1D peaks when considering all data versus data from smaller sections of a fault (e.g., Haddon et al., 2016; N. Han et al., 2018; Ren et al., 2016). For example, Ren et al. (2016) found COPD peaks in multiples of 5 m on neighboring fault sections, but those peaks correspond to different numbers of earthquakes and thus do not record the same slip history. To account for this limitation, some authors do 1D COPD analyses for interpreted fault sections (e.g., Haddon et al., 2016; Kurtz et al., 2018; Ren et al., 2016). The downside of this approach is that rupture endpoints of paleo earthquakes are usually unknown and may not be correctly interpreted from fault structure (Wesnousky, 2006) due to rupture of partial fault sections (Schwartz, 2018).

2D probability density methods with sufficiently small spatial bins help address this limitation because the large number of spatial bins allows for spatially variable slip history without explicit interpretation of paleo-rupture endpoints. From modern ruptures where fault sections and rupture endpoints are known, we find that ~20% of the modern surface ruptures considered have bi-modal 1D COPD curves when analyzing the full rupture, but using 2D COPD methods may show differences in slip history from neighboring fault sections. The Mw7.1

Ridgecrest earthquake provides a modern example (Figure 3c). A 1D COPD of the surface rupture has a peak at 0.6 m, missing the high slip zone in the middle of the rupture, but the 2D methods highlight the high slip zone and varying slip characteristics of the surface rupture. Similarly, 2D methods illustrate different slip histories at the ends of the Fuyun fault (Figure 4c) and places where sparse data have an outsize effect on 1D peak values on the Karakax fault (Figure 4a). These examples highlight the superior performance of 2D methods over 1D in interpreting paleo-slip distributions.

5.2. Characteristic Slip and the Regularity of COPD Peaks

Most studies that use COPD methods argue for characteristic slip on the studied fault or fault section (Figure 8c and Table 1). Characteristic slip is the same distribution and amplitude of slip in each earthquake on a fault or fault section; whereas characteristic earthquakes are similar-sized maximum earthquakes on a fault (Schwartz & Coppersmith, 1984; Sieh, 1996; Wesnousky et al., 1983). The presence or absence of characteristic earthquakes cannot be determined from probability density analysis of offset geomorphic markers because geomorphic markers do not record earthquake size; they record the amount of slip. Here we discuss only characteristic slip.

We review the literature to assess the prevalence of characteristic slip reported by prior studies. We analyze the likelihood of characteristic slip for a fault by reading the authors' interpretation of their data for all 29 studies that present geomorphic evidence of multiple earthquakes, defining bins based on the authors' language (Table 1). Of the 29 studies included in this analysis, 22 of them discuss the possibility of characteristic slip in the manuscript text. Our interpretation of the authors' statements in the text of those 22 studies is that characteristic slip is unlikely in three studies; allowable in six; likely in four; and unquestionably supported in nine (Figure 8c and Table 1). Most authors consider the entire studied fault, although a few consider individual fault sections separately. Some authors use the term "semi-characteristic" slip to explain the patterns they observe, but there is not an agreed-upon value of $CV_{slip-per-event}$ that constitutes characteristic (or semi-characteristic) slip. This is evident in the minimal correlation between stated support for characteristic or semi-characteristic slip and $CV_{slip-per-event}$ values as reported in the study or calculated from their data. The studies that unquestionably advocate for characteristic slip have $CV_{slip-per-event}$ values of 0.04–0.35; likely characteristic slip $CV_{slip-per-event}$ values are 0.06–0.42; and possible $CV_{slip-per-event}$ values range from 0.09 to 0.25.

In contrast to the frequent support for characteristic slip from geomorphic data, mean slip-per-event at a point calculated from paleoseismic sites on strike-slip faults is more variable. The average of $CV_{slip-per-event}$ values for 58 individual paleoseismic sites on strike-slip faults is 0.50 ± 0.06 (1σ) (Hecker et al., 2013), although many of these sites include only two or three earthquakes. This is in contrast to the lower mean $CV_{slip-per-event}$ values calculated herein and from published studies for geomorphic offset data (0.24–0.41).

This mismatch between the paleoseismic and geomorphic records has been reported previously (Zielke, 2018) and is observed on individual faults where there is enough data for comparison. At Wallace Creek on the San Andreas Fault, slip varies from 1.4 to 8 m per earthquake in the last six earthquakes from paleoseismic studies (Liu et al., 2004), with a $CV_{slip-per-event}$ of 0.43, whereas $CV_{slip-per-event}$ from geomorphic data is 0.09 (Zielke et al., 2010). On the Haiyuan fault, Ren et al. (2016) report that based on geomorphic offset data they might conclude that the Haiyuan fault experiences characteristic slip, but the paleoseismic trenching data disagrees. This mismatch between the variability of slip-at-a-point from paleoseismic sites and the suggested prevalence of characteristic slip from COPD analysis implies that COPD peaks may not represent the entire slip history.

If COPD peaks do not accurately record slip history, what do they record, and what makes them anomalously regular? One possibility is that peaks in a 1D COPD analysis combine offset measurements from different earthquakes that result from the natural variability in slip along strike (e.g., Zielke, 2018). Small measurements from older earthquakes (such as at the tails of ruptures) are combined with large measurements from more recent events (Figure 6). In this way, the 1D COPD method smooths through natural variability resulting from different earthquakes, and in the process creates peaks that are more self-similar.

A second possibility is that the resolution of displacement in paleoseismic trenches is greater than in the geomorphic record (e.g., Zielke, 2018). To explain the mismatch between paleoseismic and geomorphic data for the Carrizo segment of the San Andreas Fault, Zielke et al. (2012) argues that the paleoseismic record in trenches records both moderate and large events, and the geomorphic record only preserves large events. Our test of non-characteristic slip history supports this idea. We found that when small-slip earthquakes follow large-slip earthquakes, slip in the smaller events must be at least half as big as the larger slip to be recorded as separate COPD peaks when variability is ≥20% (Figure 11). Thus, earthquakes that break the surface with small slip may not be recorded by individual COPD peaks.

A third possibility is that offset peaks record climate events in addition to tectonic slip. Work on the Bidart fan on the San Andreas Fault indicates that regional channel incision events are less frequent than earthquakes (Grant Ludwig et al., 2010). Thus, even the smallest displacements recorded by offset channels may integrate slip from multiple earthquakes, and COPD peaks derived from those offset measurements would include multiple earthquakes per peak. On the contrary, if channel incision events occur more frequently than earthquakes, such as on the Garlock fault (McGill & Sieh, 1991) and other low-strain-rate faults, then the smallest offsets record slip from the most recent event and COPD analysis may be valid to interpret individual earthquake slip. Finally, recent work has shown that the mean annual precipitation rate of a region affects the distribution of offset sizes recorded by channels along strike-slip faults (Reitman et al., 2023), with wetter regions more likely to have large channels that record many slip events and drier regions more likely to have small channels that may record individual earthquakes, another indication that COPD peaks reflect a combination of tectonic and climate signals.

Taken together, these lines of evidence indicate that COPD peaks only record individual earthquake slip when all ruptures on the studied fault section are full-length ruptures with minimal slip variability, geomorphic marker formation is more frequent than earthquake recurrence, and all surface-rupturing earthquakes have large surface slip. When these conditions are not met, COPD peaks integrate slip from multiple earthquakes. The reported prevalence of characteristic slip in the geomorphic record (Figure 8, Table 1) thus likely relies on COPD peaks that integrate slip from multiple earthquakes.

5.3. Conditions Required to Preserve Multiple Slip Distributions

Faults that satisfy certain conditions may record more than two paleo-slip distributions. From the real and synthetic data sets analyzed here, we infer that faults or fault sections with ≤30% slip variability, at least ∼3 m slip-per-event, smaller earthquakes with slip-per-event ≥50% the slip-per-event of larger earthquakes, and high data density (at least ∼40 offset measurements at 30% noise) are more likely to preserve more than two paleo-slip distributions. Additionally, a semi-arid climate is necessary to preserve multiple sizes of cumulative offsets (Reitman et al., 2023). Finally, surface ruptures must have minimal distributed deformation to preserve robust slip distributions because distributed deformation is unlikely to be recorded by offset markers because small strain over a large area is more difficult to identify and measure (e.g., Rockwell et al., 2002) and more easily eroded and altered. Faults with site-specific data may offer a better record of multiple earthquakes because, for example, trench investigations can act as bounds to guide interpretation of slip history from a 2D COPD (e.g., N. Han et al., 2018; Ren et al., 2016; Zielke et al., 2012). However, extrapolation along strike remains a challenge because the endpoints of paleo ruptures may be uncertain (Schwartz, 2018; Wesnousky, 2006). Given these conditions, faults with an optimal combination of large slip-per-event, low slip variability, and semi-arid climate are more likely to preserve multiple paleo-slip distributions, but they are the exception.

6. Conclusion

This work examines how surface ruptures on strike-slip faults are stored in the geomorphic record and interpreted with cumulative offset probability distribution (COPD) analysis methods. Using offset measurement data from modern strike-slip surface ruptures, faults with geomorphic evidence of multiple earthquakes, and numerical simulations of offset measurements, we find that:

1. The geomorphic record generally does not resolve more than two paleo-slip distributions for strike-slip faults, except in specific cases with low slip variability, high slip-per-event, and climatic conditions that preserve multiple generations of offset markers.
2. Three studies with different approaches (Lin et al., 2020; Zielke 2018, this study) all conclude that the geomorphic record only resolves 2–3 1D density peaks at typical slip variability.
3. 1D density peaks do approximate average slip-per-event for most modern strike-slip surface ruptures, and at least 40–50 non-correlated offset measurements are needed to get an accurate 1D density peak with 30% along-strike variability.

4. For non-characteristic slip history, surface slip in smaller earthquakes must be at least 50% the amplitude of surface slip in larger earthquakes to be recorded as a separate 1D COPD peak (with 20% along-strike variability).
5. Characteristic slip may be less common than interpreted from the geomorphic record.

Finally, we propose that 2D analysis methods are used in addition to 1D to interpret slip history, and that a set of interpreted slip distributions are constructed to define uncertainty bounds and explore different possible interpretations of paleo-slip distribution.

Data Availability Statement

Modern surface rupture slip distribution data are from Reitman (2021). Geomorphic offset data are from Reitman, Klinger, et al. (2022) and in the original publications cited in Table 1. A computational notebook to apply these methods to offset measurement data is available from (Reitman et al., 2024). Any use of trade, firm, or product names is for descriptive purposes only and does not imply endorsement by the U.S. Government.

Acknowledgments
NGR, RWB, and RDG are supported by the U.S. Geological Survey Earthquake Hazards Program. NGR acknowledges support from the Université Paris Cité visiting researcher program. We thank Michele Cooke, Devin McPhillips, and Olaf Zielke for their constructive reviews.

References

Akyüz, H. S., Hartleb, R., Barka, A., Altunel, E., Sunal, G., Meyer, B., & Armijo, R. (2002). Surface rupture and slip distribution of the 12 November 1999 Düzce earthquake (M 7.1), North Anatolian fault, Bolu, Turkey. *Bulletin of the Seismological Society of America*, *92*(1), 61–66. https://doi.org/10.1785/0120000840

Ansberque, C., Bellier, O., Godard, V., Lasserre, C., Wang, M., Braucher, R., et al. (2016). The Longriqu fault zone, eastern Tibetan Plateau: Segmentation and Holocene behavior. *Tectonics*, *35*(3), 565–585. https://doi.org/10.1002/2015TC004070

Antoine, S. L., Klinger, Y., Delorme, A., Wang, K., Bürgmann, R., & Gold, R. D. (2021). Diffuse deformation and surface faulting distribution from submetric image correlation along the 2019 Ridgecrest, California, ruptures. *Bulletin of the Seismological Society of America*, *111*(5), 2275–2302. https://doi.org/10.1785/0120210036

Arrowsmith, J. R., & Rhodes, D. D. (1994). Original forms and initial modifications of the Galway Lake Road scarp formed along the Emerson fault during the 28 June 1992 Landers, California, earthquake. *Bulletin of the Seismological Society of America*, *84*(3), 511–527.

Baize, S., Nurminen, F., Sarmiento, A., Dawson, T., Takao, M., Scotti, O., et al. (2019). A worldwide and unified database of surface ruptures (SURE) for fault displacement hazard analyses. *Seismological Research Letters*, *91*(1), 499–520. https://doi.org/10.1785/0220190144

Benjelloun, Y., de Sigoyer, J., Garambois, S., Carcaillet, J., & Klinger, Y. (2021). Segmentation and Holocene behavior of the middle strand of the North Anatolian fault (NW Turkey). *Tectonics*, *40*(11), 1–32. https://doi.org/10.1029/2021tc006870

Bi, H., Zheng, W., Lei, Q., Zeng, J., Zhang, P., Chen, G., & Chen, G. (2020). Surface slip distribution along the West Helanshan fault, Northern China, and its implications for fault behavior. *Journal of Geophysical Research: Solid Earth*, *125*(7), 1–20. https://doi.org/10.1029/2020JB019983

Bi, H., Zheng, W., Zhang, P., Zeng, J., Shao, Y., Yao, Y., et al. (2022). Recovering surface slip distribution along the Sertengshan Piedmont fault (Northern China) from airborne LiDAR data. *Tectonics*, *41*(8), e2021TC007174. https://doi.org/10.1029/2021TC007174

Chen, T., Liu-Zeng, J., Shao, Y., Zhang, P., Oskin, M. E., Lei, Q., & Li, Z. (2018). Geomorphic offsets along the creeping Laohu Shan section of the Haiyuan fault, northern Tibetan Plateau. *Geosphere*, *14*(3), 1165–1186. https://doi.org/10.1130/GES01561.1

De Pascale, G. P., Quigley, M. C., & Davies, T. R. (2014). Lidar reveals uniform Alpine fault offsets and bimodal plate boundary rupture behavior, New Zealand. *Geology*, *42*(5), 411–414. https://doi.org/10.1130/G35100.1

DuRoss, C. B., Gold, R. D., Dawson, T. E., Scharer, K. M., Kendrick, K. J., Sinan, O., et al. (2020). Surface displacement distributions for the July 2019 Ridgecrest, California, earthquake ruptures. *Bulletin of the Seismological Society of America*, *110*(4), 1400–1418. https://doi.org/10.1785/0120200058

Elliott, A. J., Oskin, M. E., Liu-Zeng, J., & Shao, Y. (2015). Rupture termination at restraining bends: The last great earthquake on the Altyn Tagh Fault. *Geophysical Research Letters*, *42*(7), 2164–2170. https://doi.org/10.1002/2015GL063107

Gold, P. O., Oskin, M. E., Elliott, A. J., Hinojosa-Corona, A., Taylor, M. H., Kreylos, O., & Cowgill, E. (2013). Coseismic slip variation assessed from terrestrial lidar scans of the El Mayor–Cucapah surface rupture. *Earth and Planetary Science Letters*, *366*, 151–162. https://doi.org/10.1016/j.epsl.2013.01.040

Gold, R. D., DuRoss, C. B., & Barnhart, W. D. (2021). Coseismic surface displacement in the 2019 Ridgecrest earthquakes: Comparison of field measurements and optical image correlation results. *Geochemistry, Geophysics, Geosystems*, *22*(3), 1–22. https://doi.org/10.1029/2020GC009326

Gold, R. D., Reitman, N. G., Briggs, R. W., Barnhart, W. D., Hayes, G. P., & Wilson, E. (2015). On- and off-fault deformation associated with the September 2013 Mw 7.7 Balochistan earthquake: Implications for geologic slip rate measurements. *Tectonophysics*, *660*(September 2013), 65–78. https://doi.org/10.1016/j.tecto.2015.08.019

Grant Ludwig, L., Akciz, S. O., Noriega, G. R., Zielke, O., & Arrowsmith, J. R. (2010). Climate-modulated channel incision and rupture history of the San Andreas fault in the Carrizo Plain. *Science*, *327*(5969), 1117–1119. https://doi.org/10.1126/science.1182837

Guo, P., Han, Z., Dong, S., Yuan, R., & Xie, Z. (2019). Surface rupture and slip distribution along the Lenglongling fault in the NE Tibetan Plateau: Implications for faulting behavior. *Journal of Asian Earth Sciences*, *172*, 190–207. https://doi.org/10.1016/j.jseaes.2018.09.008

Haddon, E., Amos, C., Zielke, O., Jayko, A., & Burgmann, R. (2016). Surface slip during large Owens Valley earthquakes. *Geochemistry, Geophysics, Geosystems*, *17*(6), 2239–2269. https://doi.org/10.1002/2015GC006033

Haeussler, P. J., Schwartz, D. P., Dawson, T. E., Stenner, H. D., Lienkaemper, J. J., Sherrod, B. L., & Personius, S. F. (2004). Surface rupture and slip distribution of the Denali and Totschunda faults in the 3 November 2002 M 7.9 earthquake, Alaska. *Bulletin of the Seismological Society of America*, *94*(6B), S23–S52. https://doi.org/10.1785/0120040626

Han, N., Shan, X., Song, X., Ren, Z., Gong, W., Wang, Z., & Zhang, Y. (2018). Paleoseismic study on the Pingdingshan-Annanba segments of the Altyn Tagh Fault based on offset clusters. *Journal of Structural Geology*, *115*(June), 19–27. https://doi.org/10.1016/j.jsg.2018.06.020

Han, S., Li, H., Pan, J., Lu, H., Zheng, Y., Liu, D., & Ge, C. (2019). Co-Seismic surface ruptures in Qiangtang Terrane: Insight into late Cenozoic deformation of central Tibet. *Tectonophysics*, *750*(26), 359–378. https://doi.org/10.1016/j.tecto.2018.11.001

Hecker, S., Abrahamson, N. A., & Wooddell, K. E. (2013). Variability of displacement at a point: Implications for earthquake-size distribution and rupture hazard on faults. *Bulletin of the Seismological Society of America*, *103*(2A), 651–674. https://doi.org/10.1785/0120120159

Jiang, W., Zhang, J., Han, Z., Tian, T., Jiao, Q., Wang, X., & Jiang, H. (2017). Characteristic slip of strong earthquakes along the Yishu fault zone in East China evidenced by offset landforms. *Tectonics*, *36*(10), 1947–1965. https://doi.org/10.1002/2016TC004363

Kang, W., Xu, X., Oskin, M. E., Yu, G., Luo, J., Chen, G., et al. (2020). Characteristic slip distribution and earthquake recurrence along the eastern Altyn Tagh fault revealed by high-resolution topographic data. *Geosphere*, *16*(1), 392–406. https://doi.org/10.1130/GES02116.1

Klinger, Y., Avouac, J. P., Dorbath, L., Karaki, N. A., & Tisnerat, N. (2000). Seismic behaviour of the Dead Sea Fault along Araba valley, Jordan. *Geophysical Journal International*, *142*(3), 769–782. https://doi.org/10.1046/j.1365-246X.2000.00166.x

Klinger, Y., Etchebes, M., Tapponnier, P., & Narteau, C. (2011). Characteristic slip for five great earthquakes along the Fuyun fault in China. *Nature Geoscience*, *4*(6), 389–392. https://doi.org/10.1038/ngeo1158

Kurtz, R., Klinger, Y., Ferry, M., & Ritz, J.-F. (2018). Horizontal surface-slip distribution through several seismic cycles: The Eastern Bogd fault, Gobi-Altai, Mongolia. *Tectonophysics*, *734–735*, 167–182. https://doi.org/10.1016/j.tecto.2018.03.011

Li, C., Li, T., Hollingsworth, J., Zhang, Y., Qian, L., & Shan, X. (2023). Strain threshold for the formation of coseismic surface rupture. *Geophysical Research Letters*, *50*(16), e2023GL103666. https://doi.org/10.1029/2023GL103666

Li, H., Van Der Woerd, J., Sun, Z., Si, J., Tapponnier, P., Pan, J., et al. (2012). Co-seismic and cumulative offsets of the recent earthquakes along the Karakax left-lateral strike-slip fault in western Tibet. *Gondwana Research*, *21*(1), 64–87. https://doi.org/10.1016/j.gr.2011.07.025

Li, X., Li, C., Wesnousky, S. G., Zhang, P., Zheng, W., Pierce, I. K. D., & Wang, X. (2017). Paleoseismology and slip rate of the western Tianjingshan fault of NE Tibet, China. *Journal of Asian Earth Sciences*, *146*(1), 304–316. https://doi.org/10.1016/j.jseaes.2017.04.031

Lienkaemper, J. J., & Strum, T. A. (1989). Reconstruction of a channel offset in 1857(?) by the San Andreas fault near Cholame, California. *Bulletin of the Seismological Society of America*, *79*(3), 901–909. https://doi.org/10.1785/bssa0790030901

Lin, Z., Liu-Zeng, J., Weldon, R. J., Tian, J., Ding, C., & Du, Y. (2020). Modeling repeated coseismic slip to identify and characterize individual earthquakes from geomorphic offsets on strike-slip faults. *Earth and Planetary Science Letters*, *545*, 11613. https://doi.org/10.1016/j.epsl.2020.116313

Lindvall, S. C., Rockwell, T. K., & Hudnut, K. W. (1989). Evidence of prehistoric earthquakes on the Superstition Hills fault from offset geomorphic features. *Bulletin of the Seismological Society of America*, *79*(2), 342–361. https://doi.org/10.1785/BSSA0790020342

Liu, J., Klinger, Y., Sieh, K., & Rubin, C. (2004). Six similar sequential ruptures of the San Andreas fault, Carrizo plain, California. *Geology*, *32*(8), 649–652. https://doi.org/10.1130/G20478.1

Manighetti, I., Perrin, C., Dominguez, S., Garambois, S., Gaudemer, Y., Malavielle, J., et al. (2015). Recovering paleoearthquake slip record in a highly dynamic alluvial and tectonic region (Hope Fault, New Zealand) from airborne lidar. *Journal of Geophysical Research: Solid Earth*, *120*(6), 3782–3803. https://doi.org/10.1002/2014JB011787

Manighetti, I., Perrin, C., Gaudemer, Y., Dominguez, S., Stewart, N., Malavieille, J., & Garambois, S. (2020). Repeated giant earthquakes on the Wairarapa fault, New Zealand, revealed by Lidar-based paleoseismology. *Scientific Reports*, *10*(1), 1–11. https://doi.org/10.1038/s41598-020-59229-3

McGill, S. F., & Sieh, K. (1991). Surficial offsets on the central and eastern Garlock fault associated with prehistoric earthquakes. *Journal of Geophysical Research*, *96*(B13), 21597–21621. https://doi.org/10.1029/91JB02030

Milliner, C. W. D., Dolan, J. F., Hollingsworth, J., Leprince, S. S., Ayoub, F. F., & Sammis, C. G. (2015). Quantifying near-field and off-fault deformation patterns of the 1992 Mw 7.3 Landers earthquake. *Geochemistry, Geophysics, Geosystems*, *16*(5), 1577–1598. https://doi.org/10.1002/2014GC005693

Ou, Q., Kulikova, G., Yu, J., Elliott, A., Parsons, B., & Walker, R. (2020). Magnitude of the 1920 Haiyuan earthquake Reestimated using seismological and geomorphological methods. *Journal of Geophysical Research: Solid Earth*, *125*(8), e2019JB019244. https://doi.org/10.1029/2019JB019244

Petersen, M. D., Dawson, T. E., Chen, R., Cao, T., Wills, C. J., Schwartz, D. P., & Frankel, A. D. (2011). Fault displacement hazard for strike-slip faults. *Bulletin of the Seismological Society of America*, *101*(2), 805–825. https://doi.org/10.1785/0120100035

Reitman, N. G. (2021). Compilation of strike-slip fault surface displacement data from recent and historical earthquakes [Dataset]. *Zenodo*. https://doi.org/10.5281/zenodo.10798925

Reitman, N. G., Klinger, Y., Briggs, R. W., & Gold, R. D. (2022). Compilation of offset measurements and fault data for global strike-slip faults with multiple earthquakes [Dataset]. *U.S. Geological Survey Data Release*. https://doi.org/10.5066/P9HN0ABD

Reitman, N. G., Klinger, Y., Briggs, R. W., & Gold, R. D. (2023). Climatic influence on the expression of strike-slip faulting. *Geology*, *51*(1), 18–22. https://doi.org/10.1130/G50393.1

Reitman, N. G., Klinger, Y., Briggs, R. W., & Gold, R. D. (2024). Computational notebook to plot offset measurements along strike-slip faults [Dataset]. *U.S. Geological Survey Data Release*. https://doi.org/10.5066/P9UK2UQ1

Reitman, N. G., Mueller, K. J., & Tucker, G. E. (2022). Surface slip variability on strike-slip faults. *Earth Surface Processes and Landforms*, *47*(4), 908–935. https://doi.org/10.1002/esp.5294

Reitman, N. G., Mueller, K. J., Tucker, G. E., Gold, R. D., Briggs, R. W., & Barnhart, K. R. (2019). Offset channels may not accurately record strike-slip fault displacement: Evidence from landscape evolution models. *Journal of Geophysical Research: Solid Earth*, *124*(12), 13427–13451. https://doi.org/10.1029/2019JB018596

Ren, Z., Zhang, Z., Chen, T., Yan, S., Yin, J., Zhang, P., et al. (2016). Clustering of offsets on the Haiyuan fault and their relationship to paleoearthquakes. *Geological Society of America Bulletin*, *128*(1/2), 3–18. https://doi.org/10.1130/B31155.1

Rizza, M., Ritz, J.-F., Braucher, R., Vassallo, R., Prentice, C., Mahan, S., et al. (2011). Slip rate and slip magnitudes of past earthquakes along the Bogd left-lateral strike-slip fault (Mongolia). *Geophysical Journal International*, *186*(3), 897–927. https://doi.org/10.1111/j.1365-246X.2011.05075.x

Rockwell, T. K., & Klinger, Y. (2013). Surface rupture and slip distribution of the 1940 Imperial Valley earthquake, Imperial fault, southern California: Implications for rupture segmentation and dynamics. *Bulletin of the Seismological Society of America*, *103*(2A), 629–640. https://doi.org/10.1785/0120120192

Rockwell, T. K., Lindvall, S., Dawson, T., Langridge, R., Lettis, W., & Klinger, Y. (2002). Lateral offsets on surveyed cultural features resulting from the 1999 Izmit and Duzce earthquakes, Turkey. *Bulletin of the Seismological Society of America*, *92*(1), 79–94. https://doi.org/10.1785/0120000809

Salisbury, J. B., Arrowsmith, J. R., Brown, N., Rockwell, T., Akciz, S., & Ludwig, L. G. (2018). The age and origin of small offsets at Van Matre Ranch along the San Andreas Fault in the Carrizo plain, California. *Bulletin of the Seismological Society of America*, *108*(2), 639–653. https://doi.org/10.1785/0120170162

Salisbury, J. B., Haddad, D. E., Rockwell, T. K., Arrowsmith, J. R., Madugo, C., Zielke, O., & Scharer, K. (2015). Validation of meter-scale surface faulting offset measurements from high-resolution topographic data. *Geosphere*, *11*(6), 1884–1901. GES01197.1. https://doi.org/10.1130/GES01197.1

Salisbury, J. B., Rockwell, T. K., Middleton, T. J., & Hudnut, K. W. (2012). LiDAR and field observations of slip distribution for the most recent surface ruptures along the central San Jacinto fault. *Bulletin of the Seismological Society of America*, *102*(2), 598–619. https://doi.org/10.1785/0120110068

Scharer, K., Salisbury, J. B., Arrowsmith, J. R., & Rockwell, T. K. (2014). Southern San Andreas Fault evaluation field activity: Approaches to measuring small geomorphic offsets—Challenges and recommendations for active fault studies. *Seismological Research Letters*, *85*(1), 68–76. https://doi.org/10.1785/0220130108

Schwartz, D. P. (2018). Review: Past and future fault rupture lengths in seismic source characterization-the long and short of it. *Bulletin of the Seismological Society of America*, *108*(5), 2493–2520. https://doi.org/10.1785/0120160110

Schwartz, D. P., & Coppersmith, K. J. (1984). Fault behavior and characteristic earthquakes: Examples from the Wasatch and San Andreas fault zones. *Journal of Geophysical Research*, *89*(B7), 5681–5698. https://doi.org/10.1029/jb089ib07p05681

Sieh, K. (1996). The repetition of large-earthquake ruptures. *Proceedings of the National Academy of Sciences*, *93*(April), 3764–3771. https://doi.org/10.1073/pnas.93.9.3764

Vallage, A., Klinger, Y., Grandin, R., Bhat, H. S., & Pierrot-Deseilligny, M. (2015). Inelastic surface deformation during the 2013 Mw 7.7 Balochistan, Pakistan, earthquake. *Geology*, *43*(12), 1079–1082. https://doi.org/10.1130/G37290.1

Virtanen, P., Gommers, R., Oliphant, T. E., Haberland, M., Reddy, T., Cournapeau, D., et al., SciPy 1.0 Contributors. (2020). SciPy 1.0: Fundamental algorithms for scientific computing in python [Software]. *Nature Methods*, *17*(3), 261–272. https://doi.org/10.1038/s41592-019-0686-2

Wallace, R. E. (1968). Notes on stream channels offset by the San Andreas Fault, southern Coast ranges, California. In W. R. Dickinson & A. Grantz (Eds.), *Proceedings of conference on geololgic problems San Andreas fault system* (pp. 6–21). Stanford University Publications. https://doi.org/10.1017/CBO9781107415324.004

Waskom, M. L. (2021). seaborn: Statistical data visualization [Software]. *Journal of Open Source Software*, *6*(60), 3021. https://doi.org/10.21105/joss.03021

Wesnousky, S. G. (2006). Predicting the endpoints of earthquake ruptures. *Nature*, *444*(7117), 358–360. https://doi.org/10.1038/nature05275

Wesnousky, S. G. (2008). Displacement and geometrical characteristics of earthquake surface ruptures: Issues and implications for seismic-hazard analysis and the process of earthquake rupture. *Bulletin of the Seismological Society of America*, *98*(4), 1609–1632. https://doi.org/10.1785/0120070111

Wesnousky, S. G., Scholz, C. H., Shimazaki, K., & Matsuda, T. (1983). Earthquake frequency distribution and the mechanics of faulting. *Journal of Geophysical Research*, *88*(B11), 9331–9340. https://doi.org/10.1029/JB088iB11p09331

Xiong, B., & Li, X. (2020). Offset measurements along active faults based on the structure from motion method - A case study of Gebiling in the Xorkoli section of the Altyn Tagh Fault. *Geodesy and Geodynamics*, *11*(5), 1–9. https://doi.org/10.1016/j.geog.2020.05.005

Zielke, O. (2018). Earthquake recurrence and the resolution potential of tectono-geomorphic records. *Bulletin of the Seismological Society of America*, *108*(3A), 1399–1413. https://doi.org/10.1785/0120170241

Zielke, O., Arrowsmith, J. R., Ludwig, L. G., & Akçiz, S. O. (2010). Slip in the 1857 and earlier large earthquakes along the Carrizo plain, San Andreas Fault. *Science*, *327*(5969), 1119–1122. https://doi.org/10.1126/science.1182781

Zielke, O., Arrowsmith, J. R., Ludwig, L. G., & Akciz, S. O. (2012). High-resolution topography-derived offsets along the 1857 Fort Tejon earthquake rupture trace, San Andreas Fault. *Bulletin of the Seismological Society of America*, *102*(3), 1135–1154. https://doi.org/10.1785/0120110230

Zielke, O., Klinger, Y., & Arrowsmith, J. R. (2015). Fault slip and earthquake recurrence along strike-slip faults - Contributions of high-resolution geomorphic data. *Tectonophysics*, *638*(1), 43–62. https://doi.org/10.1016/j.tecto.2014.11.004

Zinke, R., Dolan, J. F., Rhodes, E. J., Van Dissen, R. J., Hatem, A. E., McGuire, C. P., et al. (2021). Latest Pleistocene–Holocene incremental slip rates of the Wairau fault: Implications for long-distance and long-term coordination of faulting between North and South Island, New Zealand. *Geochemistry, Geophysics, Geosystems*, *22*(9), 1–16. https://doi.org/10.1029/2021GC009656

Zinke, R., Hollingsworth, J., & Dolan, J. F. (2014). Surface slip and off-fault deformation patterns in the 2013 Mw 7.7 Balochistan, Pakistan earthquake: Implications for controls on the distribution of near-surface co-seismic slip. *Geochemistry, Geophysics, Geosystems*, *15*(12), 5034–5050. https://doi.org/10.1002/2014GC005538